

Supporting Information for
Towards Efficient and Unified Treatment of Static and
Dynamic Correlations in Generalized Kohn-Sham Density
Functional Theory

Yizhen Wang¹, Zihan Lin¹, Runhai Ouyang², Bin Jiang³, Igor Ying Zhang^{1,4,5†}, Xin Xu^{1,4†}

*¹Shanghai Key Laboratory of Molecular Catalysis and Innovation Materials,
Collaborative Innovation Centre of Chemistry for Energy Materials, MOE Laboratory
for Computational Physical Science, Department of Chemistry, Fudan University,
Shanghai 200438, China.*

²Materials Genome Institute, Shanghai University, Shanghai 200444, China.

*³Key Laboratory of Precision and Intelligent Chemistry, Department of Chemical
Physics, University of Science and Technology of China, Hefei, Anhui 230026, China.*

⁴Hefei National Laboratory, Hefei 230088, China.

⁵Shanghai Key Laboratory of Bioactive Small Molecules.

†Correspondence and requests for materials should be addressed to Igor Ying Zhang
(igor_zhangying@fudan.edu.cn) (I.Y.Z.), and Xin Xu (xxchem@fudan.edu.cn) (X.X.).

1. The R-xDH7 Functional.....	8
2. The SCC15 Model.....	10
3. Computational Details.....	12

The GMTKN55 dataset

The MBD23-594 dataset

The MGCDB84 dataset

The MG23 dataset

Dissociation of methanol on the Cu(111) surface

Hydrogen chains

i-FCIQMC

4. Supplementary Figures.....	17
--------------------------------------	-----------

Figure S1 | WTMAD-2 values for the Radical7 database versus WTMAD-2 for the Nonradical48 sub-database as calculated by R-xDH7, R-xDH7-SCC15 and other functionals.

Figure S2 | Change of features (χ_a , χ_b , ΔE , r_i , and ΔE_x) along the whole dissociation curves of $C_2H_6 \rightarrow CH_3 + CH_3$, $OH \rightarrow O + H$, and $H_2O \rightarrow O + 2H$.

Figure S3 | Performances of various methods in the MGCDB84 dataset.

Figure S4 | Performances of various methods on the (S1) $H_2 \rightarrow H + H$ dissociation curve. a) Calculated potential energy curves for breaking H-H bond of the H_2 molecule. b) Mean absolute errors (MAEs) of these methods in the regions of equilibrium, middle range, and dissociation limit of $H_2 \rightarrow H + H$ dissociation curve.

Figure S5 | Performances of various methods on the (S2) $C_2H_6 \rightarrow CH_3 + CH_3$ dissociation curve. a) Calculated potential energy curves for breaking C-C bond of the C_2H_6 molecule. b) Mean absolute errors (MAEs) of these methods in the regions of equilibrium, middle range, and dissociation limit of $C_2H_6 \rightarrow CH_3 + CH_3$ dissociation curve.

Figure S6 | Performances of various methods on the (S3) $F_2 \rightarrow F + F$ dissociation curve. a) Calculated potential energy curves for breaking F-F bond of the F_2 molecule. b) Mean absolute errors (MAEs) of these methods in the regions of equilibrium, middle range, and dissociation limit of $F_2 \rightarrow F + F$ dissociation curve.

Figure S7 | Performances of various methods on the (S4) $CH_4 \rightarrow CH_3 + H$ dissociation curve. a)

Calculated potential energy curves for breaking C-H bond of the CH₄ molecule. b) Mean absolute errors (MAEs) of these methods in the regions of equilibrium, middle range, and dissociation limit of CH₄ → CH₃ + H dissociation curve.

Figure S8| Performances of various methods on the (S5) NH₃ → NH₂ + H dissociation curve. a) Calculated potential energy curves for breaking N-H bond of the NH₃ molecule. b) Mean absolute errors (MAEs) of these methods in the regions of equilibrium, middle range, and dissociation limit of NH₃ → NH₂ + H dissociation curve.

Figure S9| Performances of various methods on the (S6) H₂O → OH + H dissociation curve. a) Calculated potential energy curves for breaking O-H bond of the H₂O molecule. b) Mean absolute errors (MAEs) of these methods in the regions of equilibrium, middle range, and dissociation limit of H₂O → OH + H dissociation curve.

Figure S10| Performances of various methods on the (S7) HF → H + F dissociation curve. a) Calculated potential energy curves for breaking H-F bond of the HF molecule. b) Mean absolute errors (MAEs) of these methods in the regions of equilibrium, middle range, and dissociation limit of HF → H + F dissociation curve.

Figure S11| Performances of various methods on the (S8) CH₃F → CH₃ + F dissociation curve. a) Calculated potential energy curves for breaking C-F bond of the CH₃F molecule. b) Mean absolute errors (MAEs) of these methods in the regions of equilibrium, middle range, and dissociation limit of CH₃F → CH₃ + F dissociation curve.

Figure S12| Performances of various methods on the (S9) CH₃Cl → CH₃ + Cl dissociation curve. a) Calculated potential energy curves for breaking C-Cl bond of the CH₃Cl molecule. b) Mean absolute errors (MAEs) of these methods in the regions of equilibrium, middle range, and dissociation limit of CH₃Cl → CH₃ + Cl dissociation curve.

Figure S13| Performances of various methods on the (M1) N₂ → N + N dissociation curve. a) Calculated potential energy curves for breaking N-N bond of the N₂ molecule. b) Mean absolute errors (MAEs) of these methods in the regions of equilibrium, middle range, and dissociation limit of N₂ → N + N dissociation curve.

Figure S14| Performances of various methods on the (M2) C₂ → C + C dissociation curve. a) Calculated potential energy curves for breaking C-C bond of the C₂ molecule. b) Mean absolute errors (MAEs) of these methods in the regions of equilibrium, middle range, and dissociation limit

of $C_2 \rightarrow C + C$ dissociation curve.

Figure S15| Performances of various methods on the (M3) $CH_4 \rightarrow C + 4H$ dissociation curve. a) Calculated potential energy curves for breaking four C-H bonds of the CH_4 molecule. b) Mean absolute errors (MAEs) of these methods in the regions of equilibrium, middle range, and dissociation limit of $CH_4 \rightarrow C + 4H$ dissociation curve.

Figure S16| Performances of various methods on the (M4) $NH_3 \rightarrow N + 3H$ dissociation curve. a) Calculated potential energy curves for breaking three N-H bonds of the NH_3 molecule. b) Mean absolute errors (MAEs) of these methods in the regions of equilibrium, middle range, and dissociation limit of $NH_3 \rightarrow N + 3H$ dissociation curve.

Figure S17| Performances of various methods on the (M5) $HCN \rightarrow HC + N$ dissociation curve. a) Calculated potential energy curves for breaking C-N bond of the HCN molecule. b) Mean absolute errors (MAEs) of these methods in the regions of equilibrium, middle range, and dissociation limit of $HCN \rightarrow HC + N$ dissociation curve.

Figure S18| Performances of various methods on the (M6) $PH_3 \rightarrow P + 3H$ dissociation curve. a) Calculated potential energy curves for breaking three P-H bond of the PH_3 molecule. b) Mean absolute errors (MAEs) of these methods in the regions of equilibrium, middle range, and dissociation limit of $PH_3 \rightarrow P + 3H$ dissociation curve.

Figure S19| Performances of various methods on the (M7) $H_2O \rightarrow O + 2H$ dissociation curve. a) Calculated potential energy curves for breaking two O-H bonds of the H_2O molecule. b) Mean absolute errors (MAEs) of these methods in the regions of equilibrium, middle range, and dissociation limit of $H_2O \rightarrow O + 2H$ dissociation curve.

Figure S20| Performances of various methods on the (M8) $H_2S \rightarrow S + 2H$ dissociation curve. a) Calculated potential energy curves for breaking two S-H bond of the H_2S molecule. b) Mean absolute errors (MAEs) of these methods in the regions of equilibrium, middle range, and dissociation limit of $H_2S \rightarrow S + 2H$ dissociation curve.

Figure S21| Performances of various methods on the (O1) $CH_3 \rightarrow CH_2 + H$ dissociation curve. a) Calculated potential energy curves for breaking C-H bond of the CH_3 radical. b) Mean absolute errors (MAEs) of these methods in the regions of equilibrium, middle range, and dissociation limit of $CH_3 \rightarrow CH_2 + H$ dissociation curve.

Figure S22| Performances of various methods on the (O2) $NH_2 \rightarrow NH + H$ dissociation curve. a)

Calculated potential energy curves for breaking N-H bond of the NH₂ radical. b) Mean absolute errors (MAEs) of these methods in the regions of equilibrium, middle range, and dissociation limit of NH₂ → NH + H dissociation curve.

Figure S23| Performances of various methods on the (O3) CH₂ → CH + H dissociation curve. a) Calculated potential energy curves for breaking C-H bond of the CH₂ molecule. b) Mean absolute errors (MAEs) of these methods in the regions of equilibrium, middle range, and dissociation limit of CH₂ → CH + H dissociation curve.

Figure S24| Performances of various methods on the (O4) NH → N + H dissociation curve. a) Calculated potential energy curves for breaking N-H bond of the NH radical. b) Mean absolute errors (MAEs) of these methods in the regions of equilibrium, middle range, and dissociation limit of NH → N + H dissociation curve.

Figure S25| Performances of various methods on the (O5) OH → O + H dissociation curve. a) Calculated potential energy curves for breaking O-H bond of the OH radical. b) Mean absolute errors (MAEs) of these methods in the regions of equilibrium, middle range, and dissociation limit of OH → O + H dissociation curve.

Figure S26| Performances of various methods on the (O6) NO → N + O dissociation curve. a) Calculated potential energy curves for breaking N-O bond of the NO molecule. b) Mean absolute errors (MAEs) of these methods in the regions of equilibrium, middle range, and dissociation limit of NO → N + O dissociation curve.

5. Supplementary Tables.....43

Table S1| Results of scsRPA, R-xDH7, R-xDH7-SCC15, B3LYP-D3BJ, PBE0-D3BJ, PBE-D3BJ, CCSD(T), XYG7 and RPA for MG23 using def2-QZVP (unit: kcal/mol). Reactions 18-21 were calculated with BSSE (Basis Set Superposition Error) correction. *Reference values of reactions 18-19 were calculated using i-FCIQMC with complete basis set extrapolated from def2-TZVP/def2-QZVP and BSSE correction, while that of reaction 20 was calculated using i-FCIQMC with def2-QZVP basis set and BSSE correction. **Reference value of reaction 15 was collected from ref. ^[1] using i-FCIQMC. (Please refer to Table S4 for more details). Other reference values were collected from refs. ^[2, 3].

Table S2| 17 chemical reactions with SCCep, SCCmb or SCC15 values exceeding 3.0 kcal/mol, filtered out from GMTKN55, MGCDB84 and MG23. *a.* taken from ref.^[2], *b.* taken from ref. ^[1], *c.*

taken from ref.^[4], *d*. taken from ref. ^[5], while *e*. calculated using i-FCIQMC with def2-QZVP basis set and BSSE correction (see Table S4).

Table S3| Results of scsRPA, R-xDH7, R-xDH7-SCC15, B3LYP-D3BJ, PBE0-D3BJ, PBE-D3BJ, CCSD(T), XYG7 and RPA for 17 chemical reactions with SCCep, SCCmb or SCC15 values exceeding 3.0 kcal/mol, filtered out from GMTKN55, MGCDB84 and MG23. *Reference values of reactions 4 and 7 were calculated using i-FCIQMC with def2-QZVP and BSSE correction.

Table S4| Reactions with updated reference values calculated by i-FCIQMC. (unit: kcal/mol) Bold numbers were chosen as the reference values in this work.

Table S5| Results of R-xDH7-SCC15, R-xDH7, B3LYP, PBE0, scsRPA, PBE, HF, XYG7, RPA and CISD at the thermodynamic limit (TDL) for the linear hydrogen chain, calculated with def2-QZVPPD. The reference values were obtained from Ref.^[6]. (unit: kcal/mol) Hydrogen chains with nearest-neighbour proton separation (bond length) *R* of 1.4, 1.6, 1.8, 2.0, 2.4, 2.8, 3.2, 3.6 bohr are studied. According to the classification used in this work, all these bond lengths are within the equilibrium region. It is difficult to obtain the self-consistent converged TDL results in the outer regions.

Table S6| Results of scsRPA, R-xDH7, R-xDH7-SCC15 for GMTKN55 (unit: kcal/mol). G21EA, G21IP, WATER27, RG18, IL16 and AHB21 were calculated with def2-QZVPPD, while other subsets were calculated with def2-QZVP.

Table S7| MADs of scsRPA, R-xDH7, R-xDH7-SCC15, XYG7, XYG3, XYGJOS, ω B97M-V, CF22D, ω B97X-V, M06-2X-D3(0), MN15-D3(BJ), B3LYP-D3(BJ), M06-D3(0), PBE0-D3(BJ) and PBE-D3(BJ) for each subset of MGCDB84 using def2-QZVPPD (unit: kcal/mol).

Table S8| Time consumption of various methods for several large species in GMTKN55 with def2-QZVP basis set. The calculations were paralleled with 36 cores of Intel® Xeon® Gold 6150 CPU @ 2.70GHz.

Table S9| Active space selection of species in different dissociation curves and parameter settings of damping function for fitting reference values.

6. Supplementary References.....60

1. The R-xDH7 Functional

$$E_{xc}^{\text{R-xDH7}} = a_1 E_x^{\text{HF}} + a_2 E_x^{\text{S}} + a_3 E_x^{\text{B88}} + a_4 E_c^{\text{VWN}} + a_5 E_c^{\text{LYP}} + a_6 E_c^{\text{osRPT2}} + a_7 E_c^{\text{ssRPT2+}}$$

Coefficients for R-xDH7:

$$a_1 = 0.9081; a_2 = 0.3600; a_3 = -0.2917;$$

$$a_4 = 0.4937; a_5 = -0.4301; a_6 = 0.8624; a_7 = 0.2359$$

The general renormalization expression of the osRPT2 correlation model is written as:

$$E_c^{\text{osRPT2}} = \sum_{\substack{\sigma=\alpha,\beta \\ \gamma \neq \sigma}} - \int_0^\infty \frac{d\omega}{2\pi} \text{Tr} [v \chi_0^\gamma(i\omega) \bar{W}^\gamma(i\omega) \chi_0^\sigma(i\omega)] = \sum_{\sigma=\alpha,\beta} E_c^{\text{osRPT2}}[\sigma]$$

where v is the bare Coulomb interaction and $\bar{W}^\gamma(i\omega)$ is a coupling-constant-averaged, frequency-dependent Coulomb interaction that is screened by γ -spin:

$$\bar{W}^\gamma(i\omega) = \int_0^1 d\lambda \frac{\lambda v}{1 - \lambda v \chi_0^\gamma(i\omega)}$$

In these equations, $\chi_0^\gamma(i\omega)$ is the frequency-dependent density response function for the γ -spin channel:

$$\chi_0^\gamma(\mathbf{r}, \mathbf{r}'; i\omega) = \sum_{ia \in \gamma} \left[\frac{\psi_i^*(r) \psi_a(r) \psi_a^*(r') \psi_i(r')}{\epsilon_i - \epsilon_a + i\omega} + c.c. \right]$$

The indices of (i and a) $\in \gamma$ are corresponded to the occupied and unoccupied γ -spin orbitals, respectively. With these definitions, the ssRPT2+ correlation is written as the difference between the standard direct RPA correlation and the osRPT2 correlation:

$$E_c^{\text{ssRPT2+}} = E_c^{\text{RPA}} - E_c^{\text{osRPT2}}$$

The osRPT2 correlation in the REST package was implemented using the resolution-of-identity (RI) approximation. Within the RI approximation, the orbital pairs are expanded with respect to a set of auxiliary basis functions:

$$\psi_i^*(r) \psi_a(r) \approx C_{ia}^u P_u(r)$$

In this context, the osRPT2 correlation in the σ -spin channel can be expressed as:

$$E_c^{\text{osRPT2}}[\sigma] = - \int_0^\infty \frac{d\omega}{2\pi} \int_0^1 d\lambda \text{Tr} \left[\Pi_\sigma(i\omega) * \left(\frac{1}{1 - \lambda * \Pi_\gamma(i\omega)} - 1 \right) \right]$$

Here $\Pi_\sigma(i\omega)$ is the response functional matrix with the matrix element defined as:

$$\Pi_\sigma(i\omega)_{\mu\nu} = \sum_i \sum_a \frac{2(\epsilon_i - \epsilon_a) C_{ia}^\mu C_{ai}^\nu}{(\epsilon_i - \epsilon_a)^2 + \omega^2}$$

The response functional radial is defined as the largest singular value of the response functional

matrix, given by

$$\chi_\sigma = \|\Pi_\sigma(i\omega)\|_2$$

In the previous work^[7], it was found that, if $\chi_\sigma > 1$, the Dyson expansion of RPA-type correlation diverges, necessitating the use of the renormalized algorithms for the evaluation of osRPA correlations.

2. The SCC15 Model

$$\text{SCC15} = \text{SCC}_{ep} + \text{SCC}_{mb}$$

$$\text{SCC}_{ep}^1 = a_1 D_1^{i=1} [b_{1-5}] + a_2 D_2^{i=1} [b_{1-5}] + a_3 D_3^{i=1} [b_{1-6}]$$

$$\text{SCC}_{ep}^i = a_4 D_4 (a_1 D_1^i [b_{1-5}] + a_2 D_2^i [b_{1-5}]) \text{ for } i > 1$$

$$\text{SCC}_{mb} = \sum_{i=5}^9 a_i D_i$$

$$D_1 = \frac{[\ln[f(r_i)]]^3}{\chi_\alpha \cdot e^{f(r_i)}} \cdot \text{erf} \left[\ln(f(r_i))^2 \right]$$

$$D_2 = \frac{[\ln[f(r_i)]]^3}{\chi_\alpha \cdot f(r_i)^{\frac{1}{3}}} \cdot \text{erf} \left[\ln(f(r_i))^2 \right]$$

$$D_3 = \frac{\Delta E_x \cdot e^{\frac{\Delta E_x}{\chi_\alpha}}}{f(r_i)} \cdot \text{erfc} \left[b_6 \cdot \frac{\Delta E_x \cdot e^{\frac{\Delta E_x}{\chi_\alpha}}}{f(r_i)} \right]$$

$$D_4 = e^{\frac{\ln(\chi_\alpha) \cdot \Delta E}{\chi_\alpha}}$$

$$D_5 = \frac{\sqrt[3]{|\chi_\alpha - \chi_\beta|}}{e^{\frac{\Delta E}{\chi_\alpha}}} \cdot \text{erf} \left[\ln(f(r_1))^4 \right]$$

$$D_6 = (\chi_\alpha - \chi_\beta) \cdot \frac{\sqrt[3]{\chi_\beta}}{\chi_\alpha \cdot e^{\Delta E}} \cdot \text{erf} \left[\ln(f(r_1))^4 \right]$$

$$D_7 = \frac{\left(\frac{E_c[\text{sCSRPA}]}{E_c[\text{PT2}]} \right)}{e^{\Delta E} \cdot e^{\sqrt[3]{\Delta E_x}}} \cdot \text{erf} \left[\ln(f(r_1))^4 \right]$$

$$D_8 = \left| \frac{\left(\frac{E_c[\text{sCSRPA}]}{E_c[\text{sBGE2}]} \right) + \left(\frac{E_c[\text{sCSRPA}]}{E_c[\text{PT2}]} \right)}{e^{\Delta E}} - \frac{\left(\frac{E_c[\text{sCSRPA}]}{E_c[\text{sBGE2}]} \right) - \left(\frac{E_c[\text{sCSRPA}]}{E_c[\text{PT2}]} \right)}{\sqrt[3]{\left(\frac{E_c[\text{sCSRPA}]}{E_c[\text{sBGE2}]} \right)}} \right| \cdot \text{erf} \left[\ln(f(r_1))^4 \right]$$

$$D_9 = \frac{(\Delta E)^2 \cdot \sqrt[3]{\Delta E_x}}{e^{\Delta E} \cdot \sqrt{\chi_\alpha}} \cdot \text{erf} \left[\ln(f(r_1))^4 \right]$$

$$f(r) = \frac{b_1 \cdot r + b_2 \cdot r^2 + b_3 \cdot r^3}{1 + b_4 \cdot r + b_5 \cdot r^2}$$

$E_c[\text{sCSRPA}]$ is the correlation energy of sCSRPA; $E_c[\text{PT2}]$ is the correlation energy of PT2;

$E_c[\text{sBGE2}]$ is the correlation energy of sBGE2.

$$a_1 = 2.5735; a_2 = -0.6688; a_3 = -0.00002756; a_4 = 0.5000;$$

$$a_5 = -0.7206; a_6 = 2.8648; a_7 = 1.5173; a_8 = -0.3992; a_9 = 0.2023;$$

$$b_1 = 0.2602; b_2 = -0.4102; b_3 = 0.1528; b_4 = -1.8257; b_5 = 0.8285; b_6 = 0.000005$$

In our newly proposed hybrid symbolic and parameter regression (HSPR) strategy, we introduced some base functional forms manually before/after the symbolic regression of SISSO. These selections were informed by their performance in addressing both dynamic and static correlation limits. It is crucial for the accuracy of the SCC model¹⁵.

- (a) **Regulation function $f(r)$** : Early in our work, we identified the sensitivity of the SCCep model to the electron-pair energy ratio. To address this, we introduced a regulation function $f(r)$ with 5 empirical parameters ($\{b_i\}$ with $i = 1$ to 5) to reshape the electron pair energy ratios $\{r_i\}$ used in the symbolic regression with the SISSO algorithm. This function was designed to maintain the same asymptotic behavior as the bare electron-pair energy ratio (r), ensuring it approaches zero in the strong correlation limit ($r = 0$) and returns to one in the dynamic correlation limit ($r = 1$).
- (b) **Error functions (erf) with respect to the logarithm of $f(r)$** : The logarithm of $f(r)$ was selected automatically by the SISSO procedure for some descriptors, indicating its effectiveness in representing the static correlation errors in various scenarios. Note that, it is particularly important to turn off the static correlation correction in the dynamic correlation limit ($r = 1$), because the logarithm of $f(r)$ approaches zero. Unfortunately, this function is problematic in the static correlation limit ($r = 0$), which diverges to $-\infty$. The error functions were thus imposed after the SISSO regression to regulate the descriptors selected in the strong correlation limit.
- (c) **The complementary error function (erfc) attached to the third descriptor (D_3)**: Same as the logarithm of $f(r)$, the inverse of $f(r)$, selected by SISSO in the D_3 descriptor, diverges in the strong correlation limit ($r = 0$). The complementary error function with one more parameter (b_6) were introduced to regulate the D_3 descriptor in the strong correlation limit.

With these pre-introduced base functions and parameters, we established a hybrid symbolic and parameter regression (HSPR) strategy, which, as described in Figure 1, optimizes these parameters non-linearly outside each SISSO procedure using the steepest descent optimization algorithm.

3. Computational Details

The GMTKN55 dataset

The GMTKN55 database, consisting of 55 subsets and encompassing a total of 1505 relative energies and 2462 molecules, is a comprehensive resource for computational chemistry^[5]. The molecular structures and the corresponding reference values were collected from the official website: “<https://www.chemie.uni-bonn.de/pctc/mulliken-center/software/GMTKN/gmtkn55>”. For this study, calculations were performed using the home-made package of Rust-based Electronic Structure Toolkit (REST), accessible via `git@github.com:igor-1982/rest.git`. Primarily, the def2-QZVP basis set^[8] was employed in the majority of these calculations. However, for specific subsets of G21EA, G21IP, WATER27, RG18, IL16 and AHB21, the def2-QZVPPD basis set^[8, 9] was utilized to ensure enhanced precision in the results.

The MBD23-594 dataset

The MBD23-594 dataset presents a comprehensive collection of dissociation curves for 23 main-group molecules, systematically categorized into three subsets: 9 close-shell single-bond dissociations (S1-S9), 8 close-shell multiple-bond dissociations (M1-M8) and 6 open-shell bond dissociations (O1-O6). In this work, calculations were performed using the REST package, except for the CCSD(T) results, which were calculated using Gaussian 16^[10]. The def2-QZVPPD basis set was employed for all calculations. The RPA results were performed based on PBE0 references. To ensure the correct electronic states along dissociation curves, the calculations with longer dissociation bond lengths were restarted from the converged density matrices of their predecessors.

We used the PySCF package^[11-13] to calculate reference values. Equilibrium regions were computed using CCSD(T)/CBS extrapolated from aug-cc-pVTZ/aug-cc-pVQZ basis sets, while areas beyond the equilibrium positions relied on NEVPT2 calculations with judiciously selected active spaces. A damping function was employed to smooth the dissociation curves calculated by CCSD(T) and NEVPT2,

$$E_{\text{ref}}(\text{dist}) = E_{\text{CCSD(T)}}(\text{dist}) \cdot \text{erf} \left[\left(A \cdot \frac{D_{\text{eq}}}{\text{dist}} \right)^n \right] + E_{\text{NEVPT2}}(\text{dist}) \cdot \left[1 - \text{erf} \left[\left(A \cdot \frac{D_{\text{eq}}}{\text{dist}} \right)^n \right] \right]$$

Table S9 summarizes the damping parameters and the active spaces used for each molecular dissociation. Subsequently, these reference values were uniformly scaled and integrated with

appropriate damping functions to represent the entire dissociation curves.

Statistical analyses were performed at different stages of the dissociation process. Statistics for the equilibrium region were derived by evaluating the local minimum point of the curves and averaging four adjacent points (two from either side). In contrast, statistics for the middle region were calculated based on the local maximum point of the R-xDH7 curves and the same pattern of adjoining four points. Finally, the dissociation limit regions were characterized using the two points with the most extended bond lengths to ensure accurate representation of the asymptotic behavior.

The MGCDB84 dataset

The MGCDB84 dataset encompasses 84 subsets containing 4986 individual data points^[4]. It is divided into 8 subsets, including NC ‘easy’ dimers (NCED, 1744 data points), NC ‘easy’ clusters (NCEC, 243 data points), NC ‘difficult’ interactions (NCD, 91 data points), ‘easy’ IEs (EIE, 755 data points), ‘difficult’ IEs (DIE, 155 data points), TC ‘easy’ (TCE, 947 data points), TC ‘difficult’ (TCD, 258 data points) and BHs (BH, 206 data points). Results of R-xDH7, R-xDH7-SCC15, scsRPA, XYG7, XYG3 and XYGJOS were calculated using the REST package and the def2-QZVPPD basis set, while the results of other methods were collected from reference [14].

The MG23 dataset

MG23 contains 23 chemical reaction energies, as shown in Supplementary Table 1. Primarily, calculations were performed using the home-made REST package, except for the CCSD(T) calculations, which were calculated using Gaussian 16^[10]. The def2-QZVP basis set was employed. The results of RPA were performed based on PBE0 references.

Dissociation of methanol on the Cu(111) surface

In the investigation of methanol dissociation in the gas phase, a comprehensive computational approach was adopted. Three distinct dissociation curves were computed utilizing the REST package for all methods, except CCSD(T), which was executed using Gaussian 16^[10]. The def2-QZVPPD basis set was employed. The RPA results were obtained based on PBE0 references.

For the periodic calculations involving PBE-D3BJ, Vienna ab initio simulation package (VASP)^[15-17] was employed. The core electrons were described by the projector augmented-wave

(PAW) method^[18]. The kinetic energy cutoff for the plane wave basis sets of the valence electrons was set to be 450 eV. The surface Monkhorst-Pack meshes^[19] of $5 \times 5 \times 1$ k-point sampling were employed. A four-layered slab was adopted to model the 4×4 supercell of Cu(111). A vacuum layer of 20 Å was added in the direction perpendicular to the surface.

In exploring the adsorption and dissociation dynamics of methanol on the Cu(111) surface, a hybrid scheme known as XO-PBC was implemented^[20-22]. This innovative methodology integrates high-level methods (H) via finite cluster models with the low-level generalized gradient approximation (L) under periodic boundary conditions (PBC). Specifically, B3LYP-D3BJ and R-xDH7-SCC15 calculations were carried out using this combined approach. The XO-PBC scheme has been extensively validated, both accuracy and efficiency in simulating numerous surface reactions of chemical interest have been proven^[20-22]. The adsorption energies using the XO-PBC formula were shown as:

$$\Delta E_{\text{XO-PBC(H:L)}}^{\text{ad}} = \Delta E_{\text{PBC@L}}^{\text{ad}} + (\Delta E_{\text{Cluster@H}}^{\text{ad}} - \Delta E_{\text{Cluster@L}}^{\text{ad}})$$

where H = B3LYP-D3BJ or R-xDH7-SCC15, and L = PBE-D3BJ in this work.

In the context of finite cluster calculations, the B3LYP-D3BJ and R-xDH7-SCC15 methods were implemented using the home-made REST package. The computational model consisted of a Cu_{31} cluster, composed of 31 copper atoms. In the recent work, we have conducted a convergence study to assess the impact of cluster size on the adsorption energy for CO on Cu(111) surfaces, as shown in Supplementary Figure 2 of Ref. 74. The results demonstrate that a cluster of 31 Cu atoms provides a good balance between computational efficiency and accuracy in capturing the short-range interactions relevant to our study of the $\text{CH}_3\text{OH-Cu(111)}$ system.^[22] For these specific finite cluster calculations, the def2-SVP basis set was employed^[23]. To guarantee that the electronic states accurately represented the molecular system throughout the entire dissociation process, the calculations with longer dissociation bond lengths were restarted from the converged density matrices of their immediate predecessors.

In a recent work (Nat. Comm. 2018, 9:4039), the potential energy surface (PES) for methanol dissociation on the Cu(111) surface has been constructed by utilizing a permutation invariant polynomial neural network (PIP-NN) and incorporating geometries optimized with the optPBE-vdW method. This approach facilitated the identification of key reaction paths, which were delineated by selecting optimal geometries along the minimum energy paths (MEPs)

predicted by the PIP-NN model. Specifically, we focused on the dissociation pathways involving O-H, C-H, and C-O bonds, ensuring a comprehensive exploration of the reaction mechanisms. The corresponding geometries on the reaction paths were attached a supporting material.

Hydrogen chain

All results were performed using the REST package, except for the CCSD(T) results, which were calculated using Gaussian 16^[10]. The def2-QZVPPD basis set was employed for all calculations. The RPA results were performed based on PBE0 references. The energies per atom in a finite cluster with N hydrogen atoms are considered: $E[N] = \frac{1}{n} E_{tot}[N]$. The thermodynamic limit (TDL) of hydrogen chain was extrapolated from the linear regression of E(N=10), E(N=20), E(N=30), E(N=40) and E(N=50), with regards to 1/N.

Statistics for the equilibrium region were derived by evaluating the local minimum point of the curves and averaging four adjacent points (two from either side). In contrast, statistics for the middle region were calculated based on the local maximum point of the R-xDH7 curves and the same pattern of adjoining four points, except that of R-xDH7-SCC15 were calculated based on the local maximum point of itself and the adjacent four points with the same pattern. Finally, the dissociation limit regions were characterized using the two points with the most extended bond lengths.

i-FCIQMC

The FCIQMC calculations were performed using the open-source code HANDE-QMC^[24]. The initiator approach (i-FCIQMC)^[25] was adopted in all FCIQMC calculations, with initiator threshold $n_a = 3.0$. The time step was automatically updated to keep the calculation stable if a bloom event was detected. The quasi-Newton approach^[26] was employed in all FCIQMC calculations for closed-shell molecules. Innermost core electrons (i.e. $1s^2$) were frozen to reduce the dimension of FCI space involved for all atoms except hydrogen. For all systems, at least 10 000 reports were used. In order to ensure the accuracy of the projected energy, the target population was adjusted to ensure that the walker population value on the reference state was at least 10^3 . With the aim of converging the calculations with respect to the target population, we have performed multiple calculations with varying target population values, for the precision

within millihartree of error margin.

4. Supplementary Figures

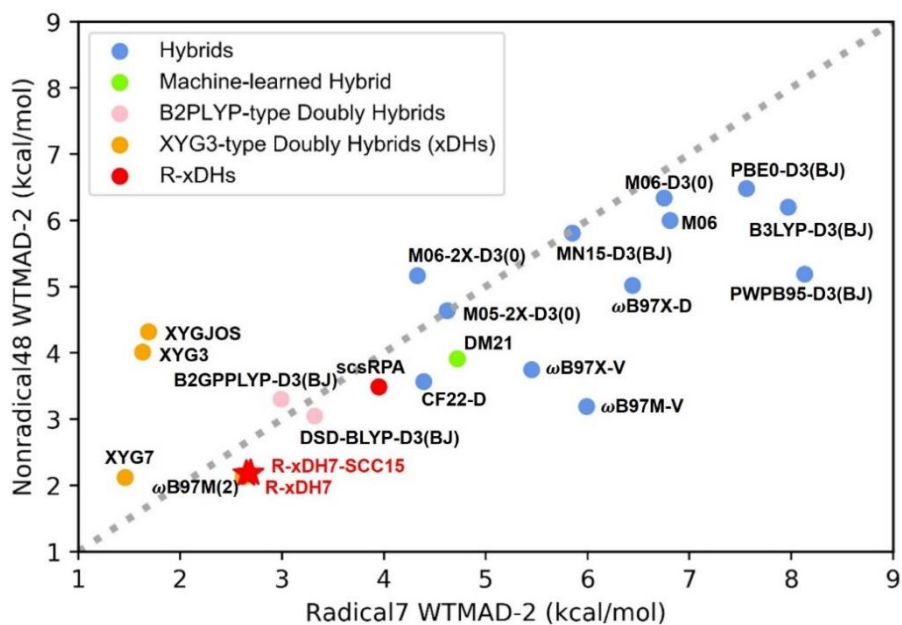


Figure S1 | WTMAD-2 values for the Radical7 sub-datasets versus WTMAD-2 for the Nonradical48 sub-datasets as calculated by R-xDH7, R-xDH7-SCC15 and other functionals.

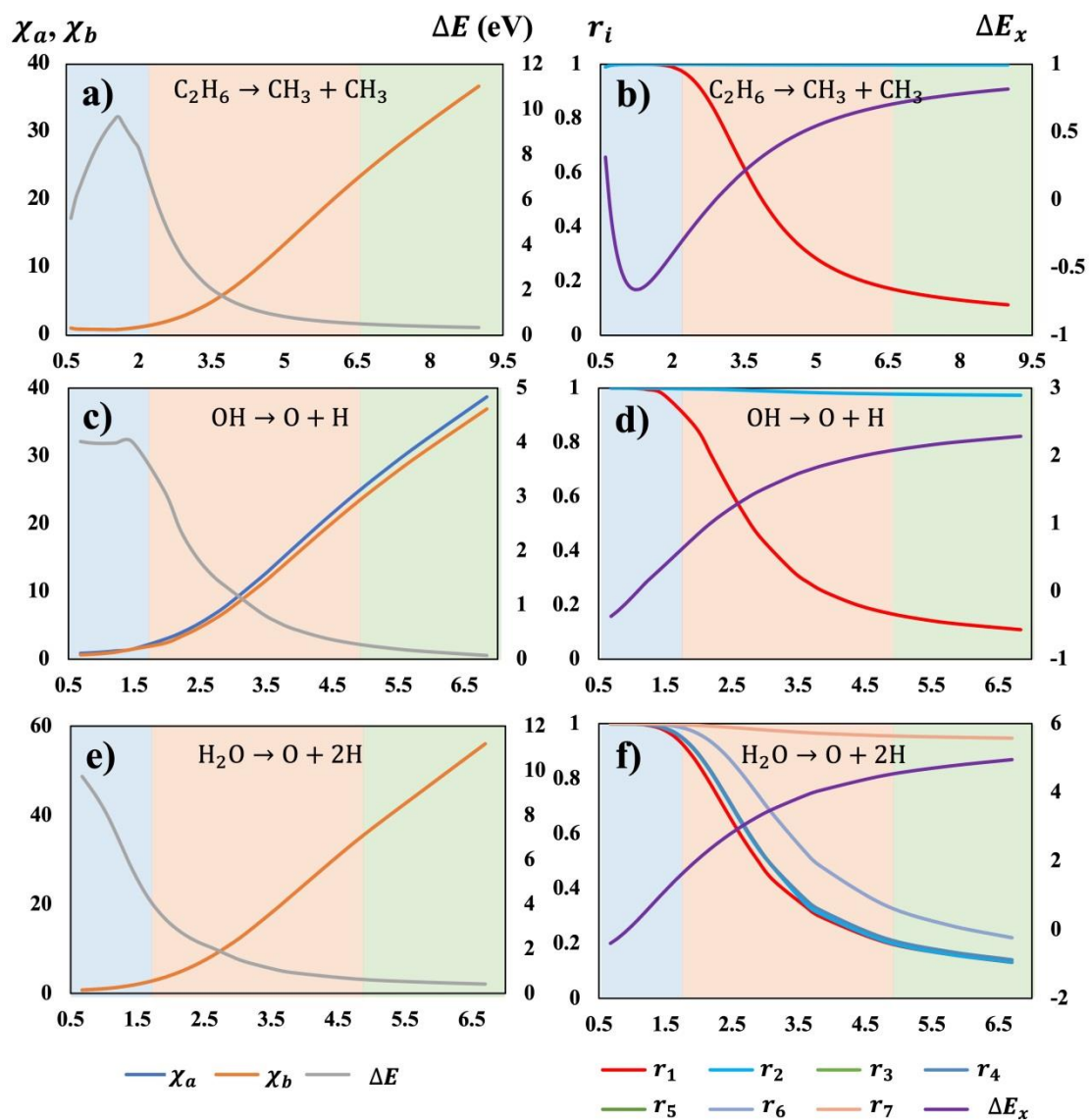


Figure S2 | Change of features (χ_a , χ_b , ΔE , r_i , and ΔE_x) along the whole dissociation curves of $\text{C}_2\text{H}_6 \rightarrow \text{CH}_3 + \text{CH}_3$, $\text{OH} \rightarrow \text{O} + \text{H}$, and $\text{H}_2\text{O} \rightarrow \text{O} + 2\text{H}$.

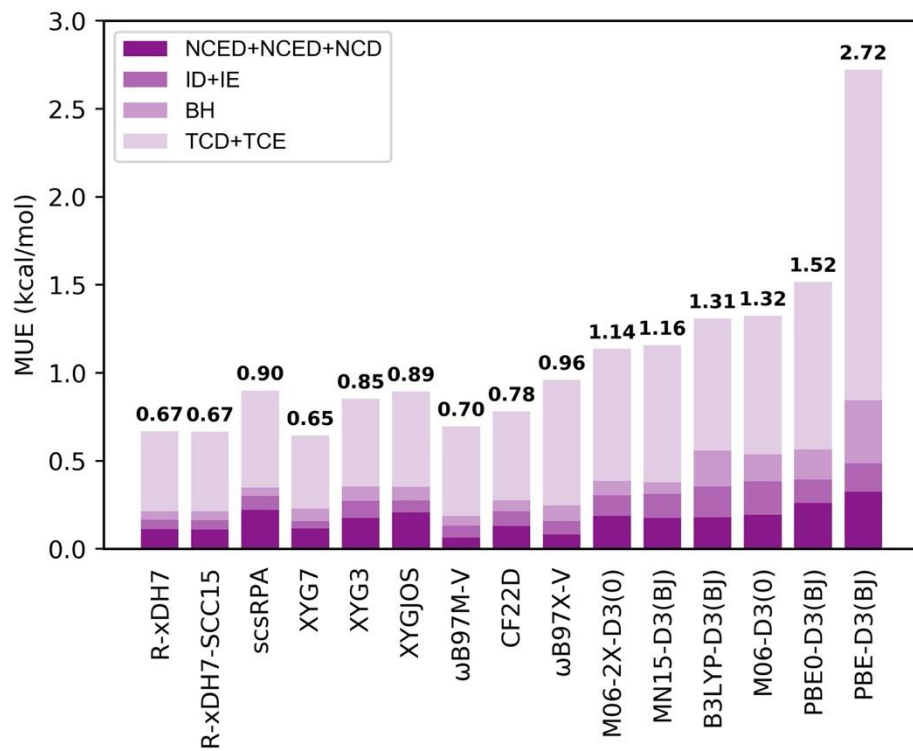


Figure S3 | Performances of various methods in the MGDCB84 dataset.

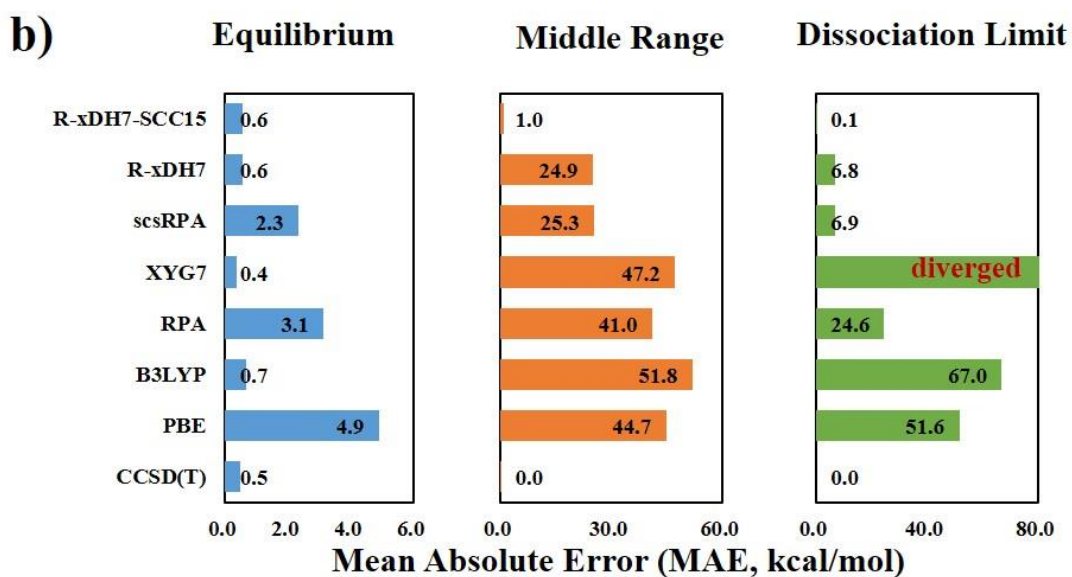
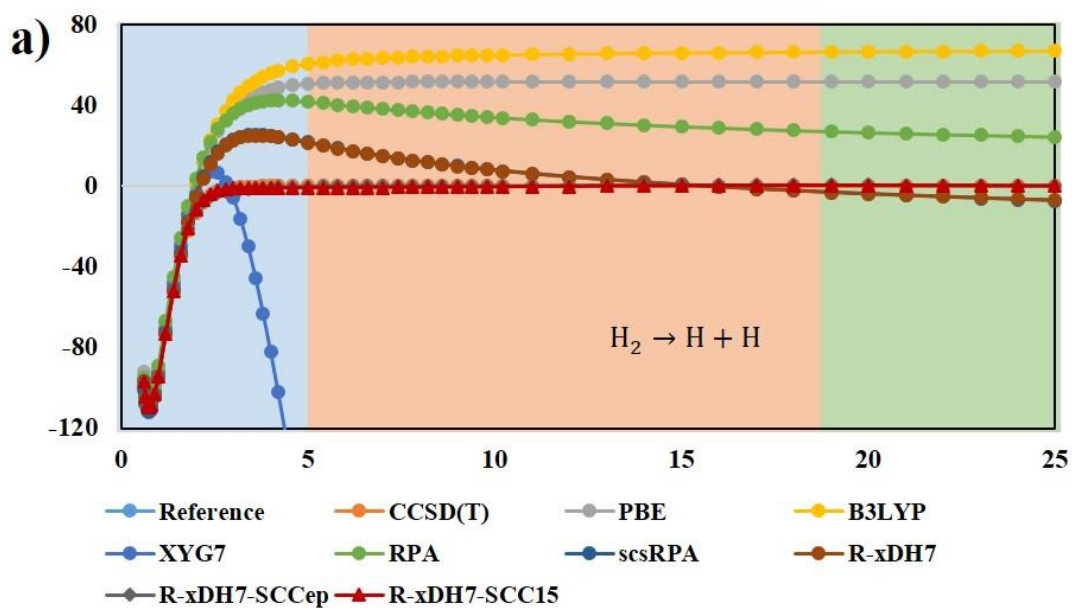


Figure S4 | Performances of various methods on the (S1) $H_2 \rightarrow H + H$ dissociation curve. a) Calculated potential energy curves for breaking H-H bond of the H_2 molecule. b) Mean absolute errors (MAEs) of these methods in the regions of equilibrium, middle range, and dissociation limit of $H_2 \rightarrow H + H$ dissociation curve.

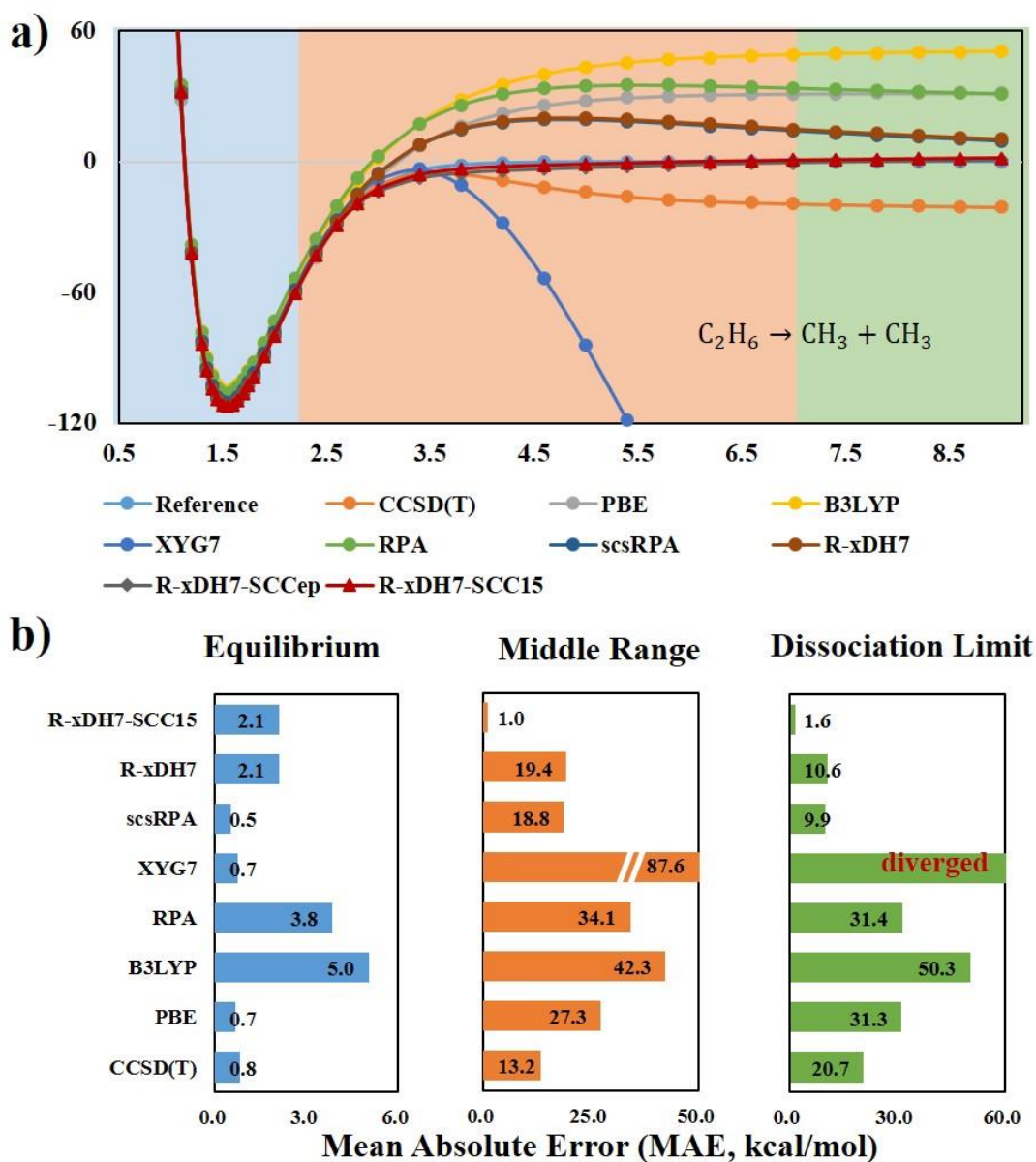


Figure S5 | Performances of various methods on the (S2) $C_2H_6 \rightarrow CH_3 + CH_3$ dissociation curve. a) Calculated potential energy curves for breaking C-C bond of the C_2H_6 molecule. b) Mean absolute errors (MAEs) of these methods in the regions of equilibrium, middle range, and dissociation limit of $C_2H_6 \rightarrow CH_3 + CH_3$ dissociation curve.

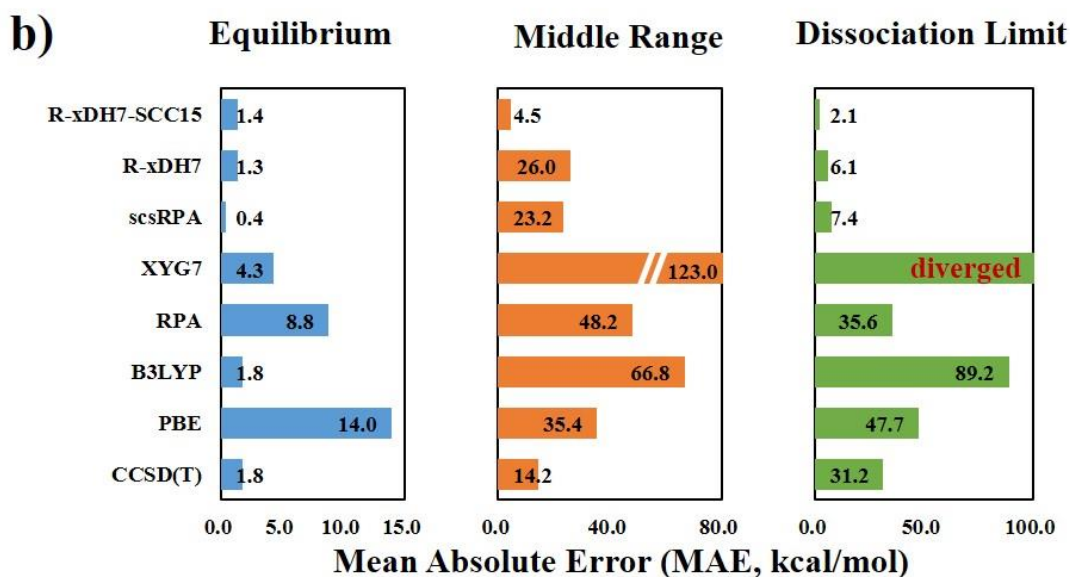
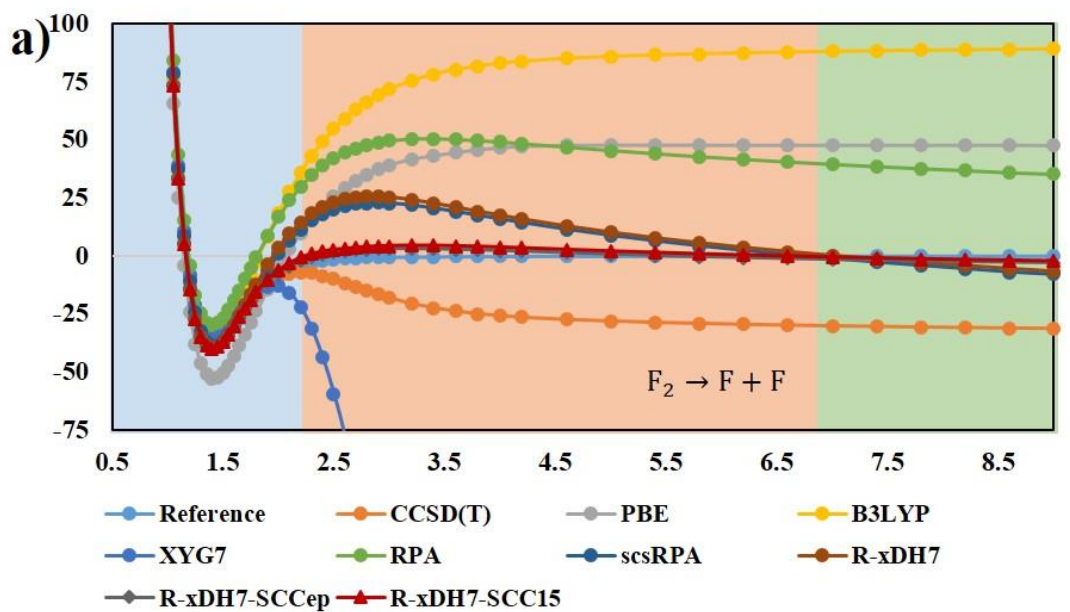


Figure S6] Performances of various methods on the (S3) $F_2 \rightarrow F + F$ dissociation curve. a) Calculated potential energy curves for breaking F-F bond of the F_2 molecule. b) Mean absolute errors (MAEs) of these methods in the regions of equilibrium, middle range, and dissociation limit of $F_2 \rightarrow F + F$ dissociation curve.

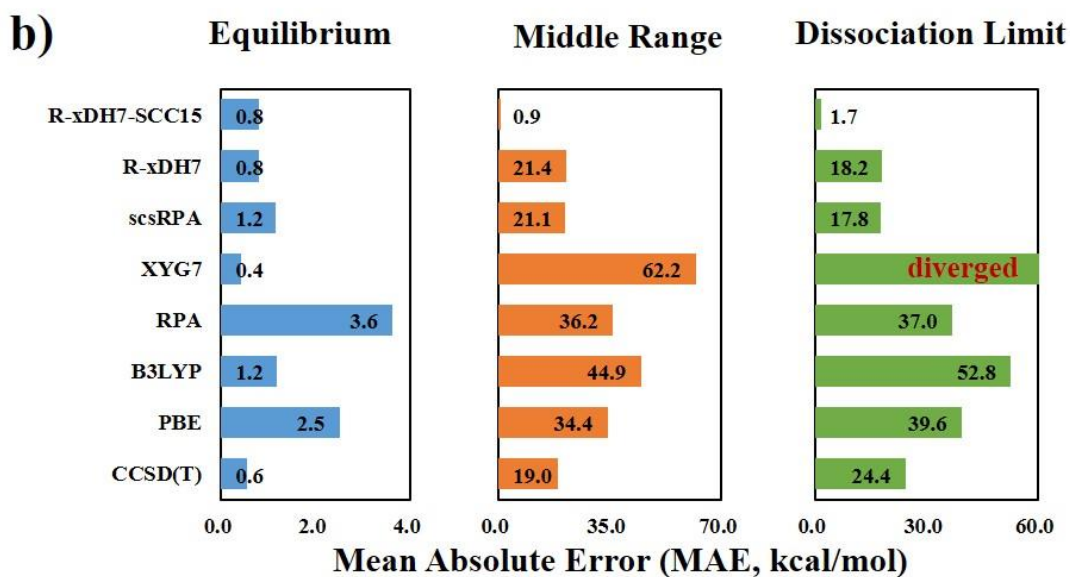
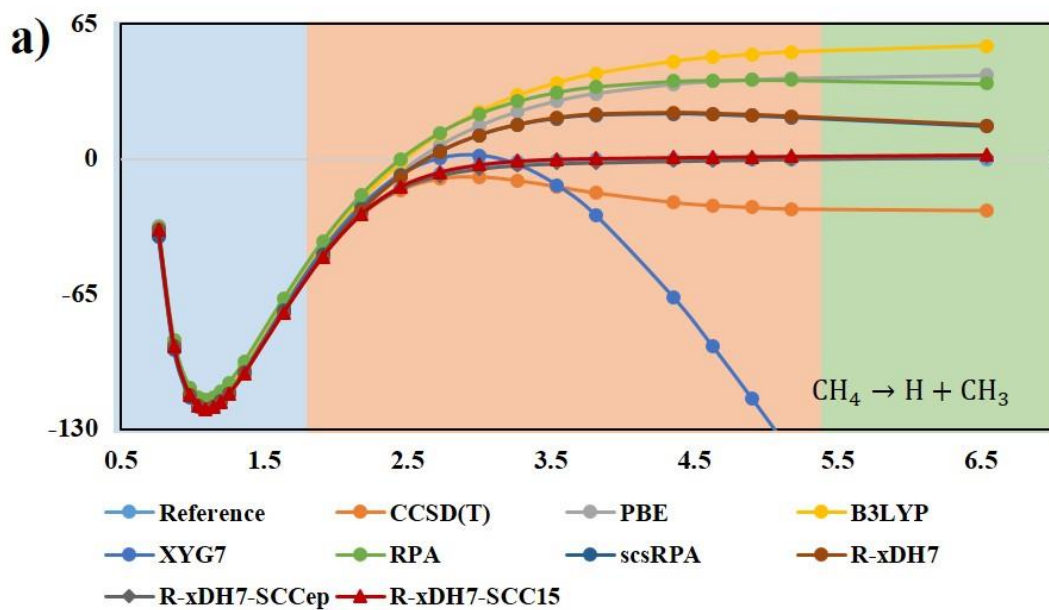


Figure S7 | Performances of various methods on the (S4) CH₄ → CH₃ + H dissociation curve. a) Calculated potential energy curves for breaking C-H bond of the CH₄ molecule. b) Mean absolute errors (MAEs) of these methods in the regions of equilibrium, middle range, and dissociation limit of CH₄ → CH₃ + H dissociation curve.

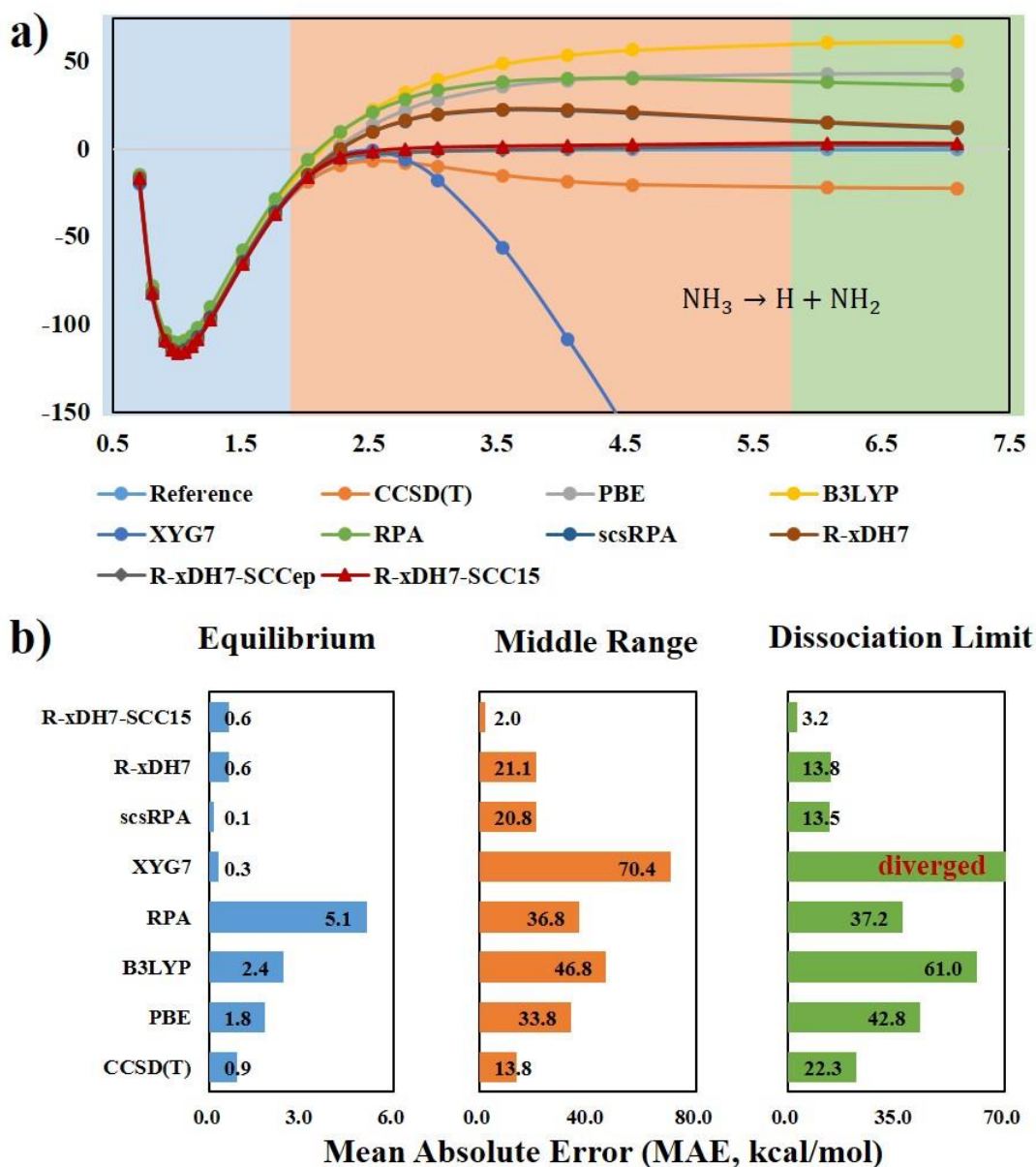


Figure S8 | Performances of various methods on the (S5) $\text{NH}_3 \rightarrow \text{NH}_2 + \text{H}$ dissociation curve. a) Calculated potential energy curves for breaking N-H bond of the NH_3 molecule. b) Mean absolute errors (MAEs) of these methods in the regions of equilibrium, middle range, and dissociation limit of $\text{NH}_3 \rightarrow \text{NH}_2 + \text{H}$ dissociation curve.

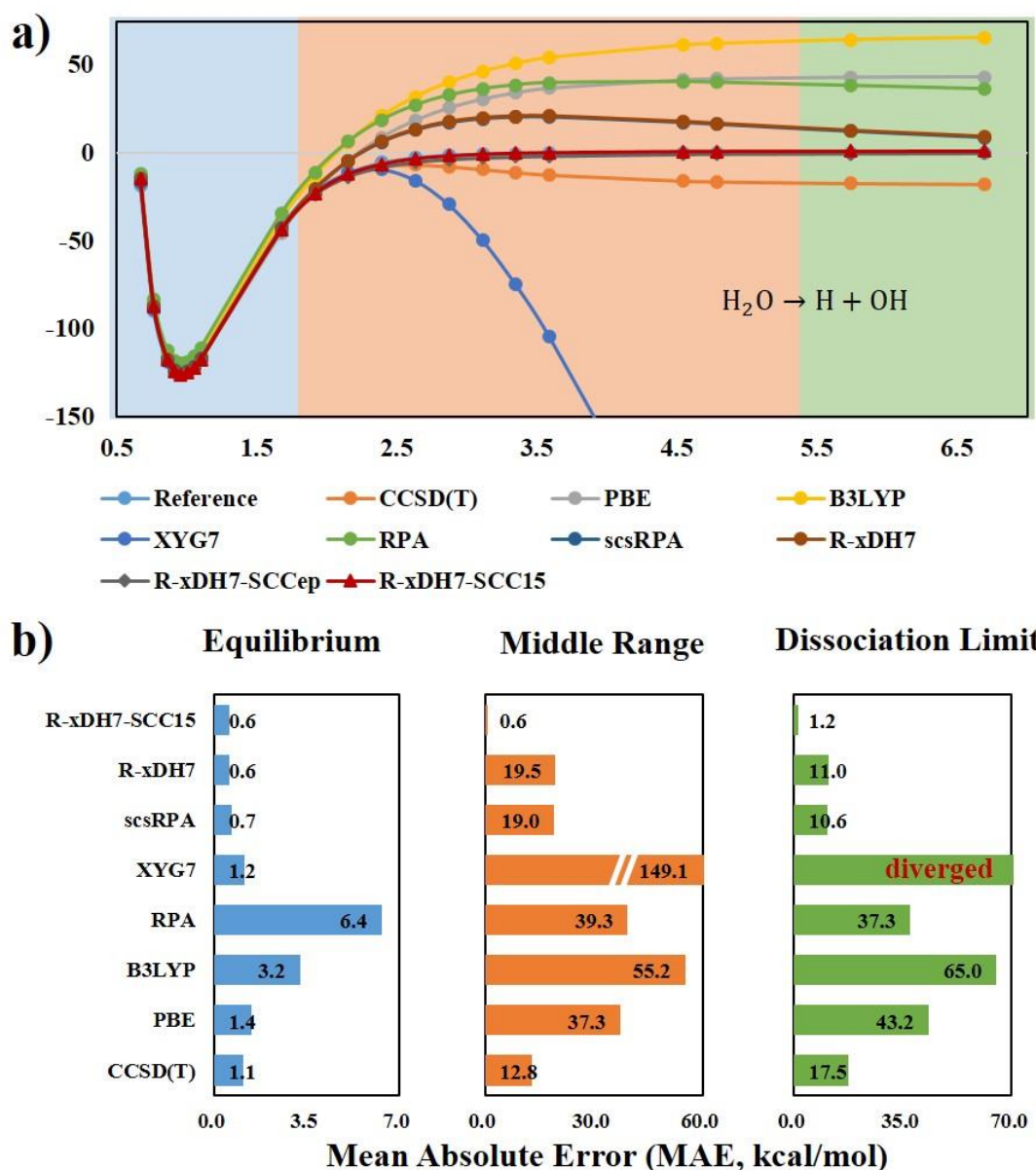


Figure S9 | Performances of various methods on the (S6) $\text{H}_2\text{O} \rightarrow \text{OH} + \text{H}$ dissociation curve. a) Calculated potential energy curves for breaking O-H bond of the H_2O molecule. b) Mean absolute errors (MAEs) of these methods in the regions of equilibrium, middle range, and dissociation limit of $\text{H}_2\text{O} \rightarrow \text{OH} + \text{H}$ dissociation curve.

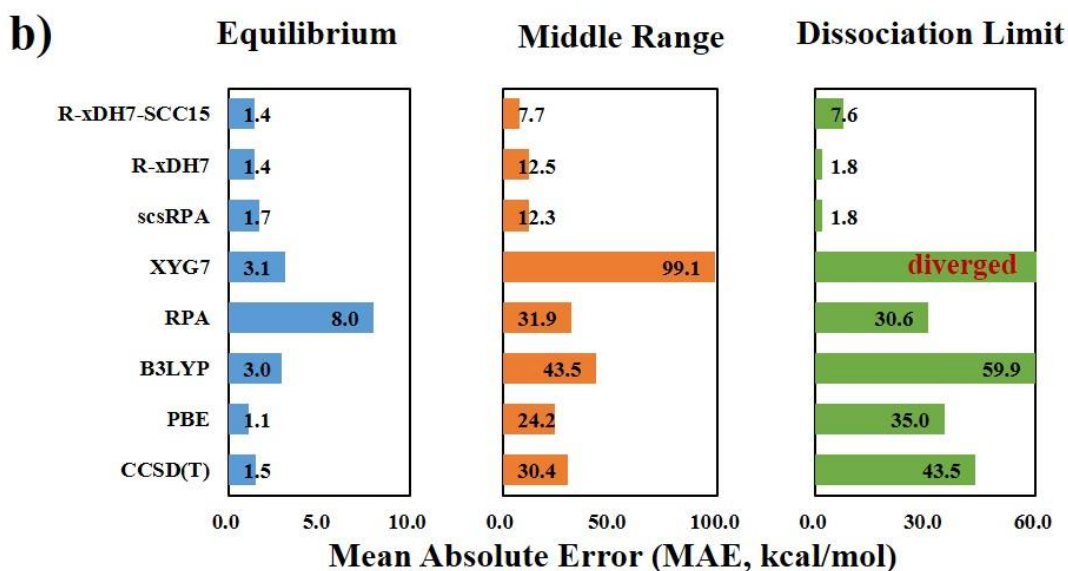
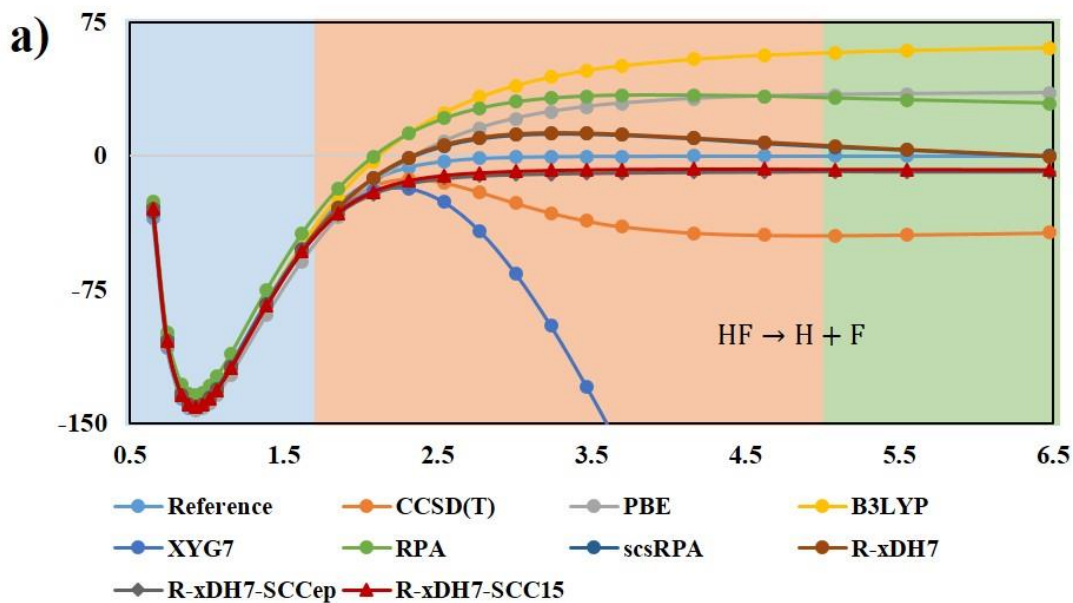
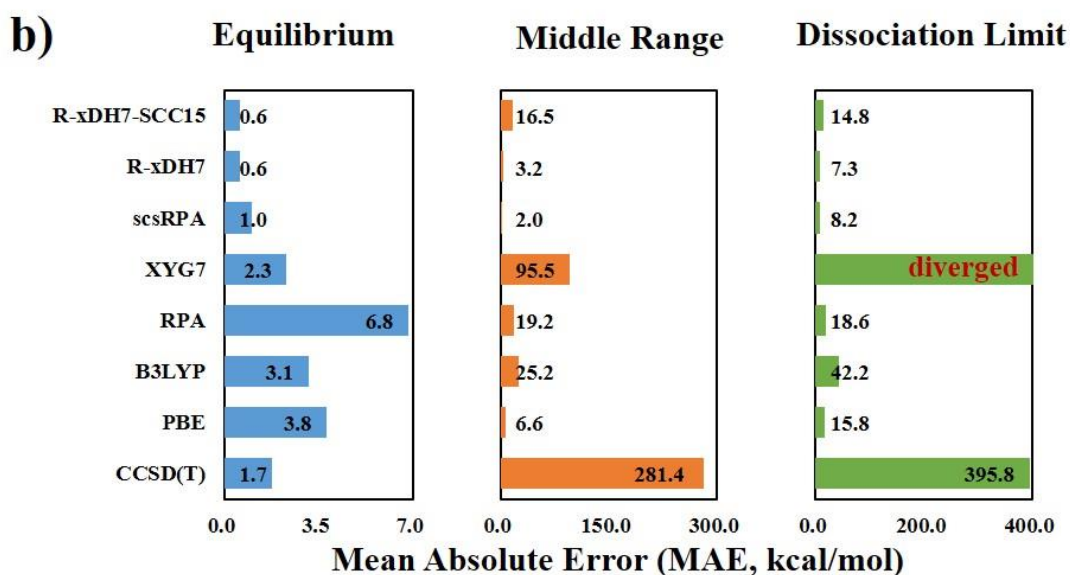
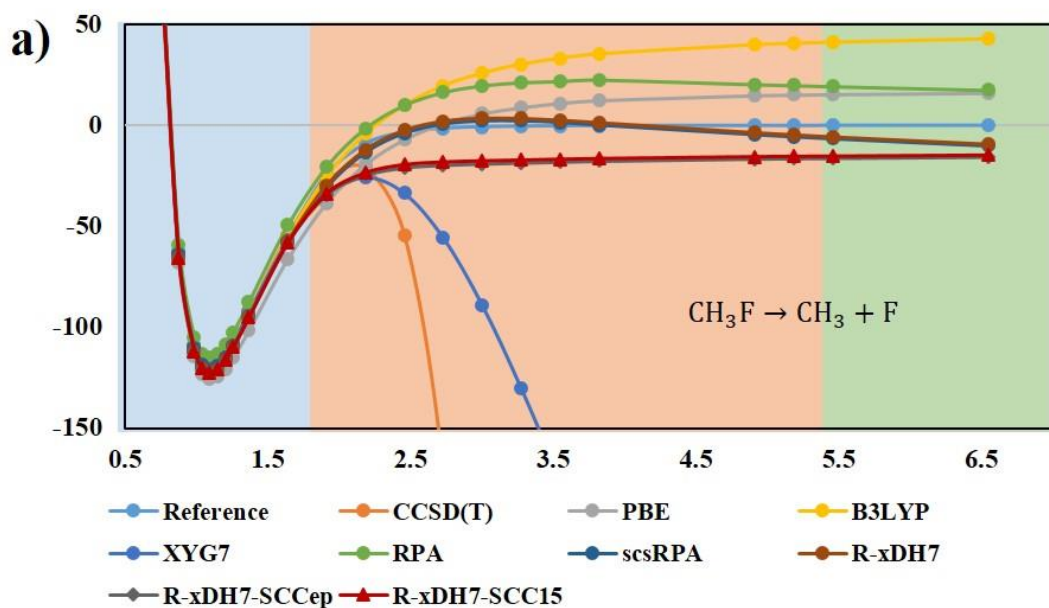
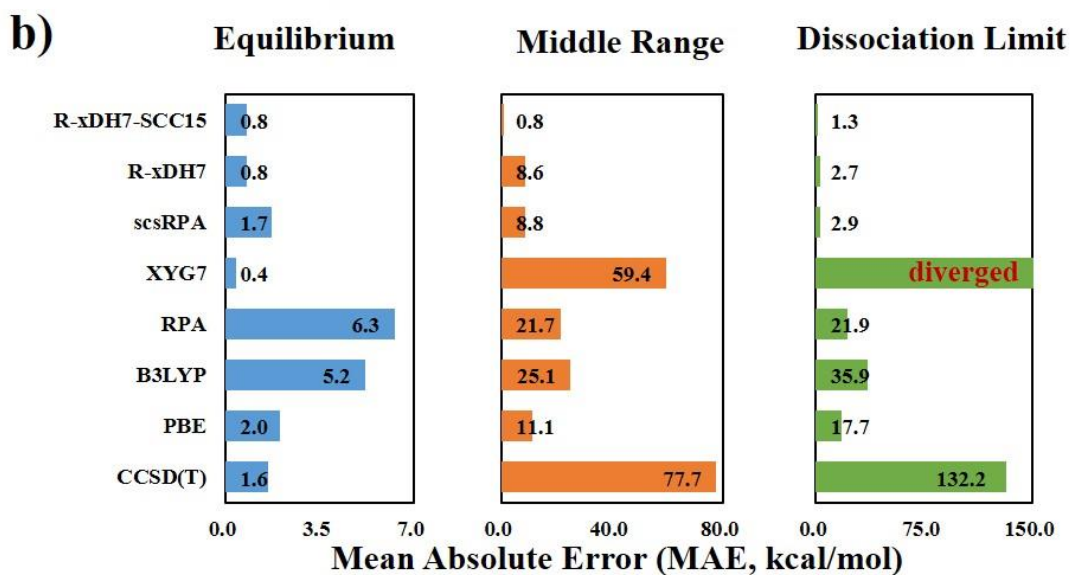
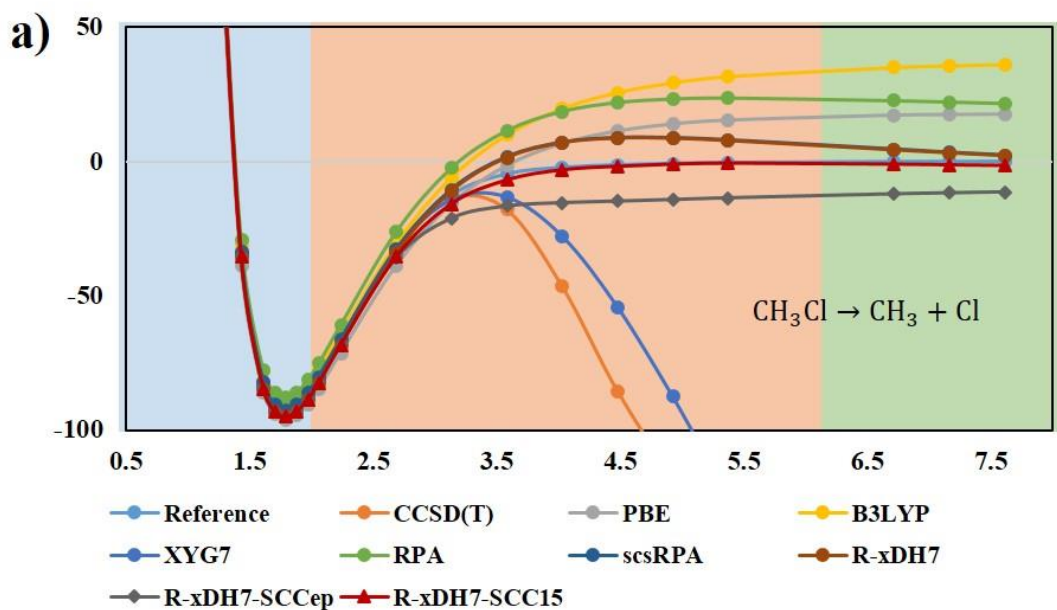


Figure S10 | Performances of various methods on the (S7) $\text{HF} \rightarrow \text{H} + \text{F}$ dissociation curve. a) Calculated potential energy curves for breaking H-F bond of the HF molecule. b) Mean absolute errors (MAEs) of these methods in the regions of equilibrium, middle range, and dissociation limit of $\text{HF} \rightarrow \text{H} + \text{F}$ dissociation curve.



*Unable to calculate the correct CCSD(T) results for bond length larger than 3.2Å.

Figure S11 | Performances of various methods on the (S8) CH₃F → CH₃ + F dissociation curve. a) Calculated potential energy curves for breaking C-F bond of the CH₃F molecule. b) Mean absolute errors (MAEs) of these methods in the regions of equilibrium, middle range, and dissociation limit of CH₃F → CH₃ + F dissociation curve.



*Unable to calculate the correct CCSD(T) results for bond length larger than 5.5 Å.

Figure S12 | Performances of various methods on the (S9) CH₃Cl → CH₃ + Cl dissociation curve. a) Calculated potential energy curves for breaking C-Cl bond of the CH₃Cl molecule. b) Mean absolute errors (MAEs) of these methods in the regions of equilibrium, middle range, and dissociation limit of CH₃Cl → CH₃ + Cl dissociation curve.

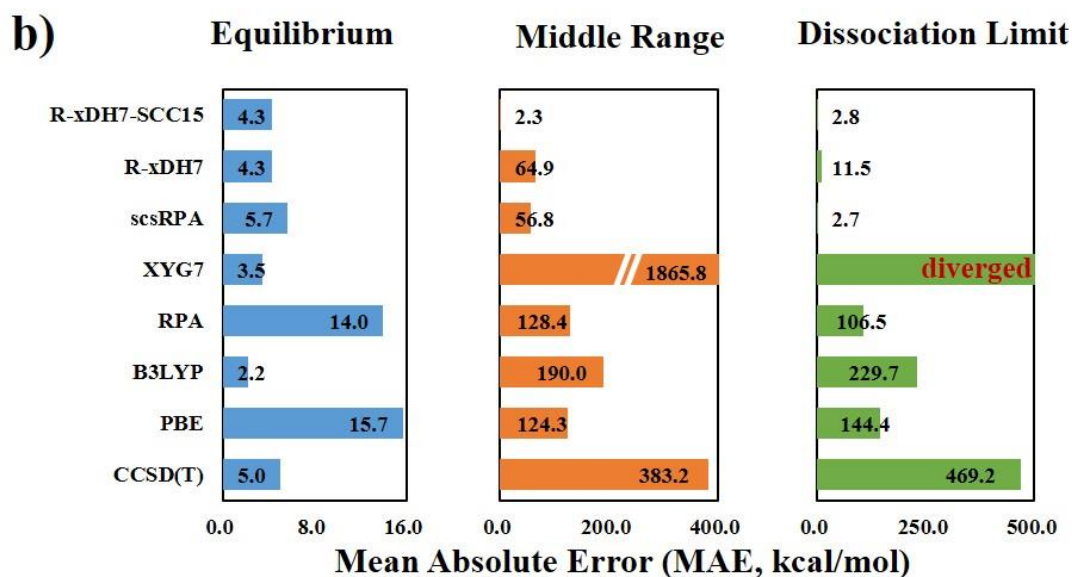
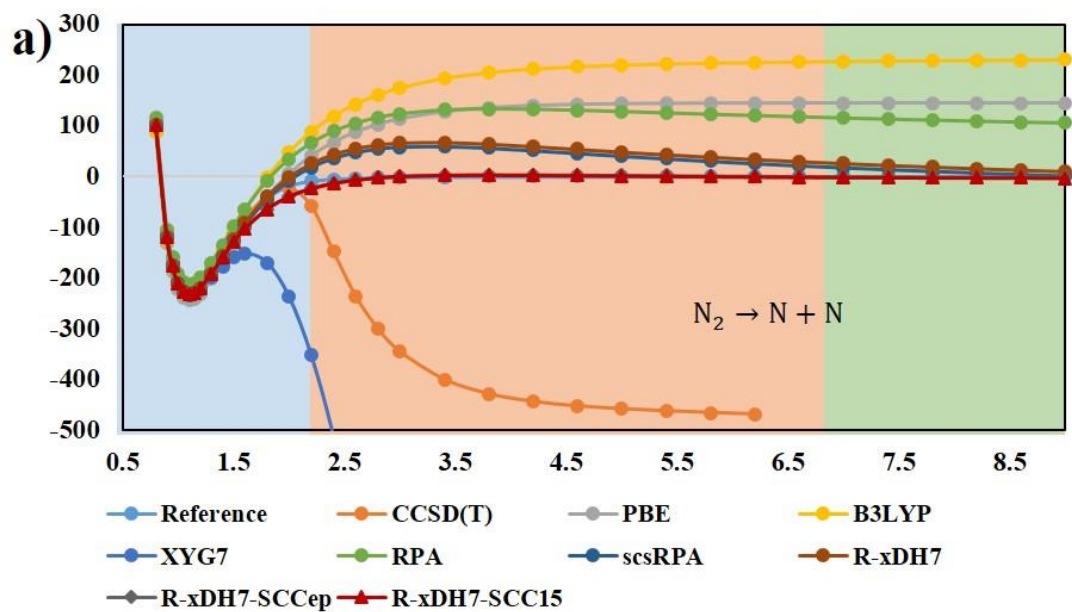


Figure S13 | Performances of various methods on the (M1) $N_2 \rightarrow N + N$ dissociation curve. a) Calculated potential energy curves for breaking N-N bond of the N_2 molecule. b) Mean absolute errors (MAEs) of these methods in the regions of equilibrium, middle range, and dissociation limit of $N_2 \rightarrow N + N$ dissociation curve.

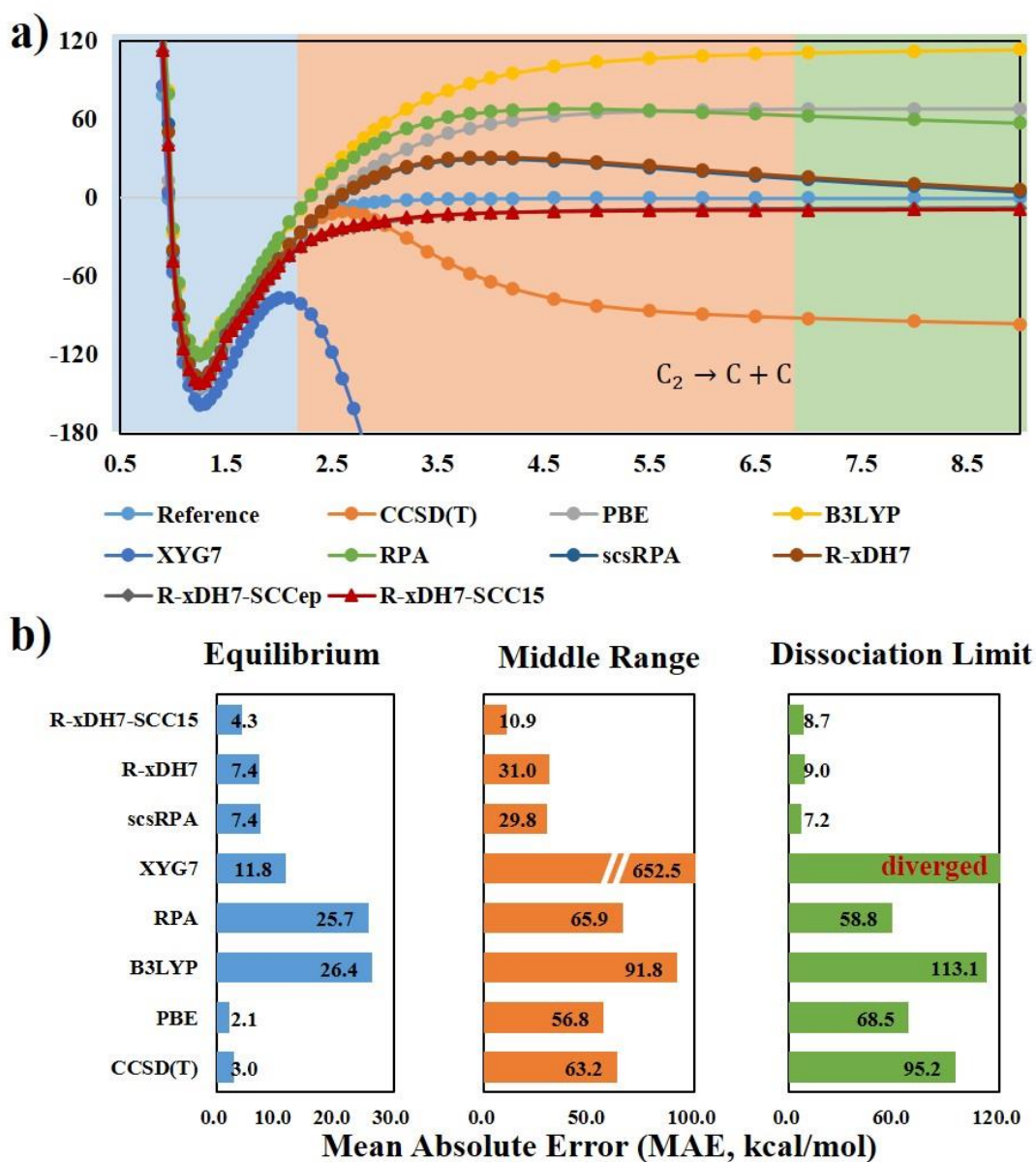


Figure S14 | Performances of various methods on the (M2) $C_2 \rightarrow C + C$ dissociation curve. a) Calculated potential energy curves for breaking C-C bond of the C_2 molecule. b) Mean absolute errors (MAEs) of these methods in the regions of equilibrium, middle range, and dissociation limit of $C_2 \rightarrow C + C$ dissociation curve.

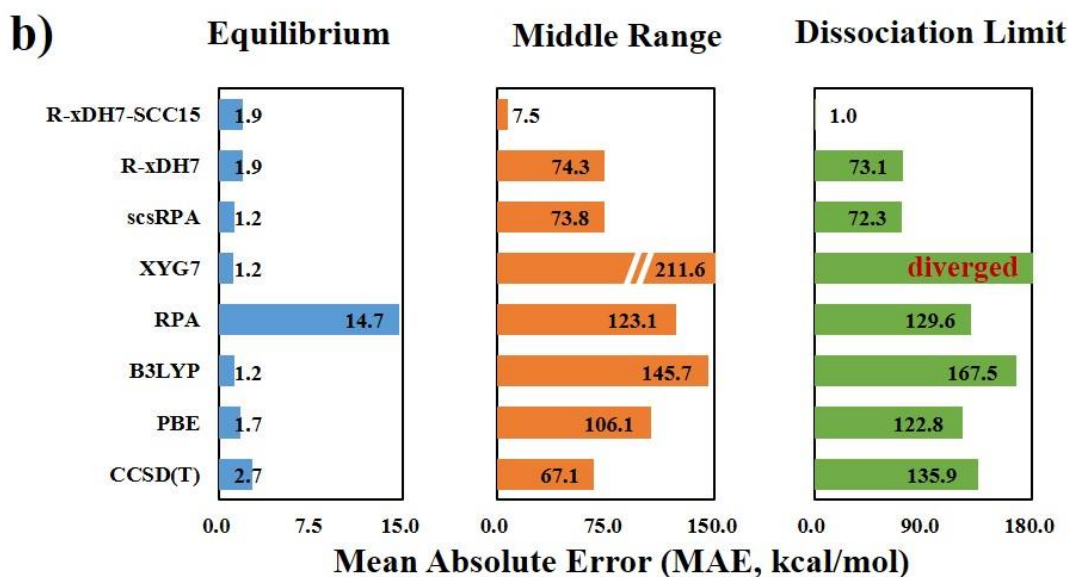
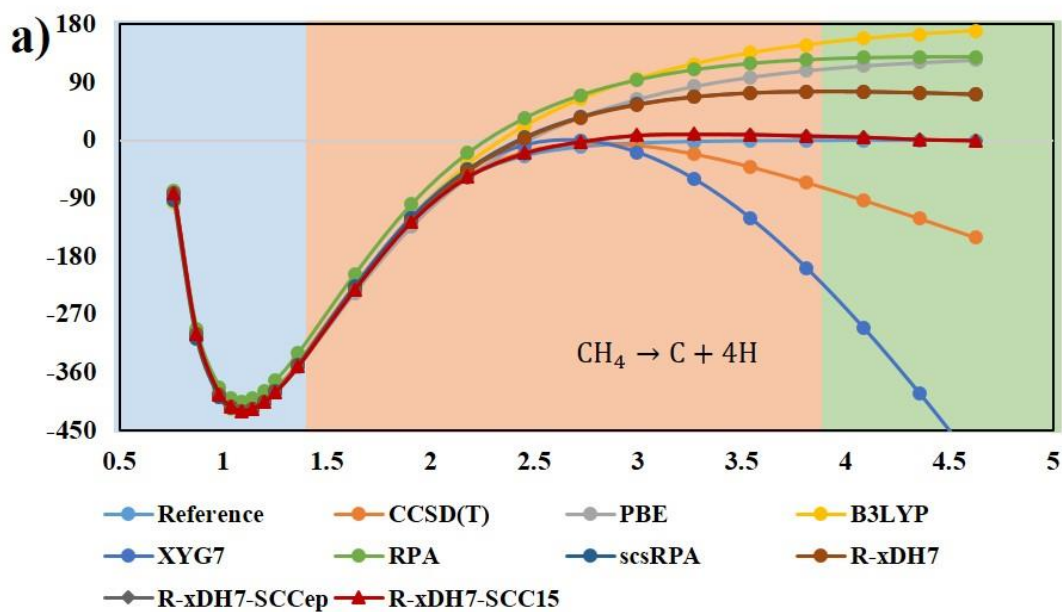


Figure S15 | Performances of various methods on the (M3) CH₄ → C + 4H dissociation curve. a) Calculated potential energy curves for breaking four C-H bonds of the CH₄ molecule. b) Mean absolute errors (MAEs) of these methods in the regions of equilibrium, middle range, and dissociation limit of CH₄ → C + 4H dissociation curve.

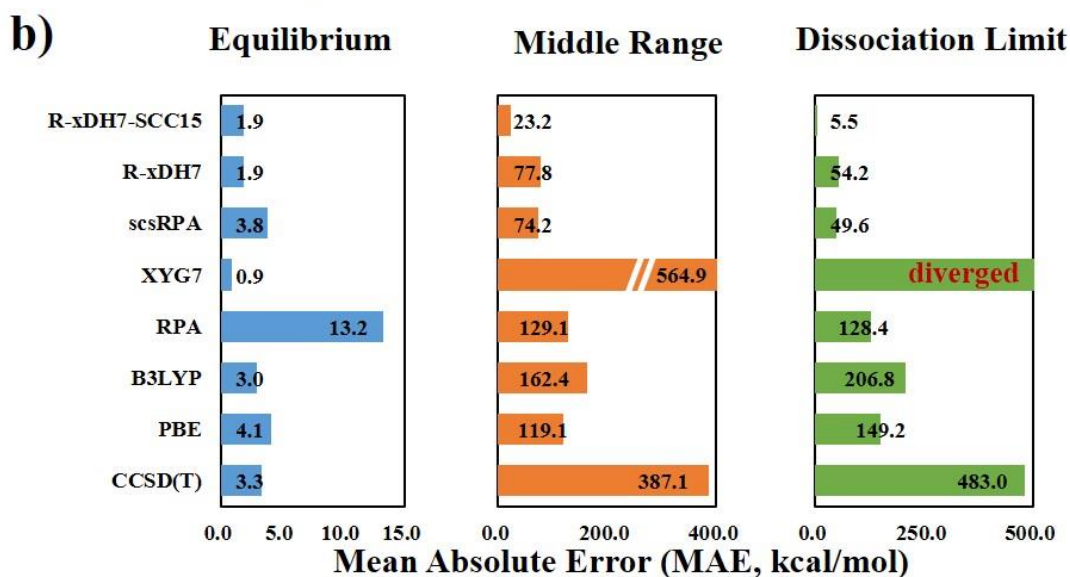
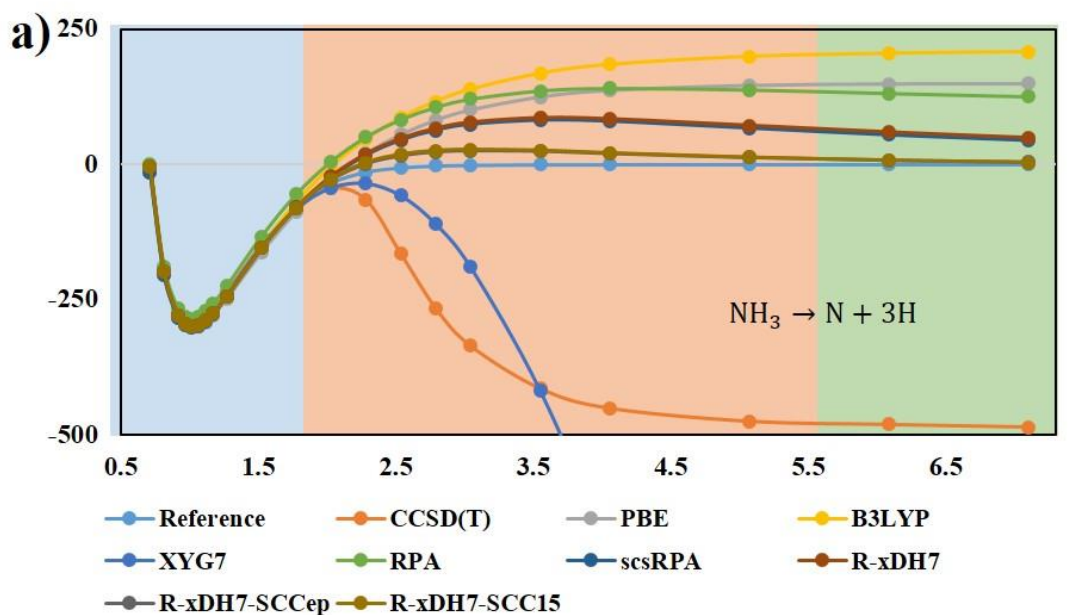


Figure S16 Performances of various methods on the (M4) $\text{NH}_3 \rightarrow \text{N} + 3\text{H}$ dissociation curve. a) Calculated potential energy curves for breaking three N-H bonds of the NH_3 molecule. b) Mean absolute errors (MAEs) of these methods in the regions of equilibrium, middle range, and dissociation limit of $\text{NH}_3 \rightarrow \text{N} + 3\text{H}$ dissociation curve.

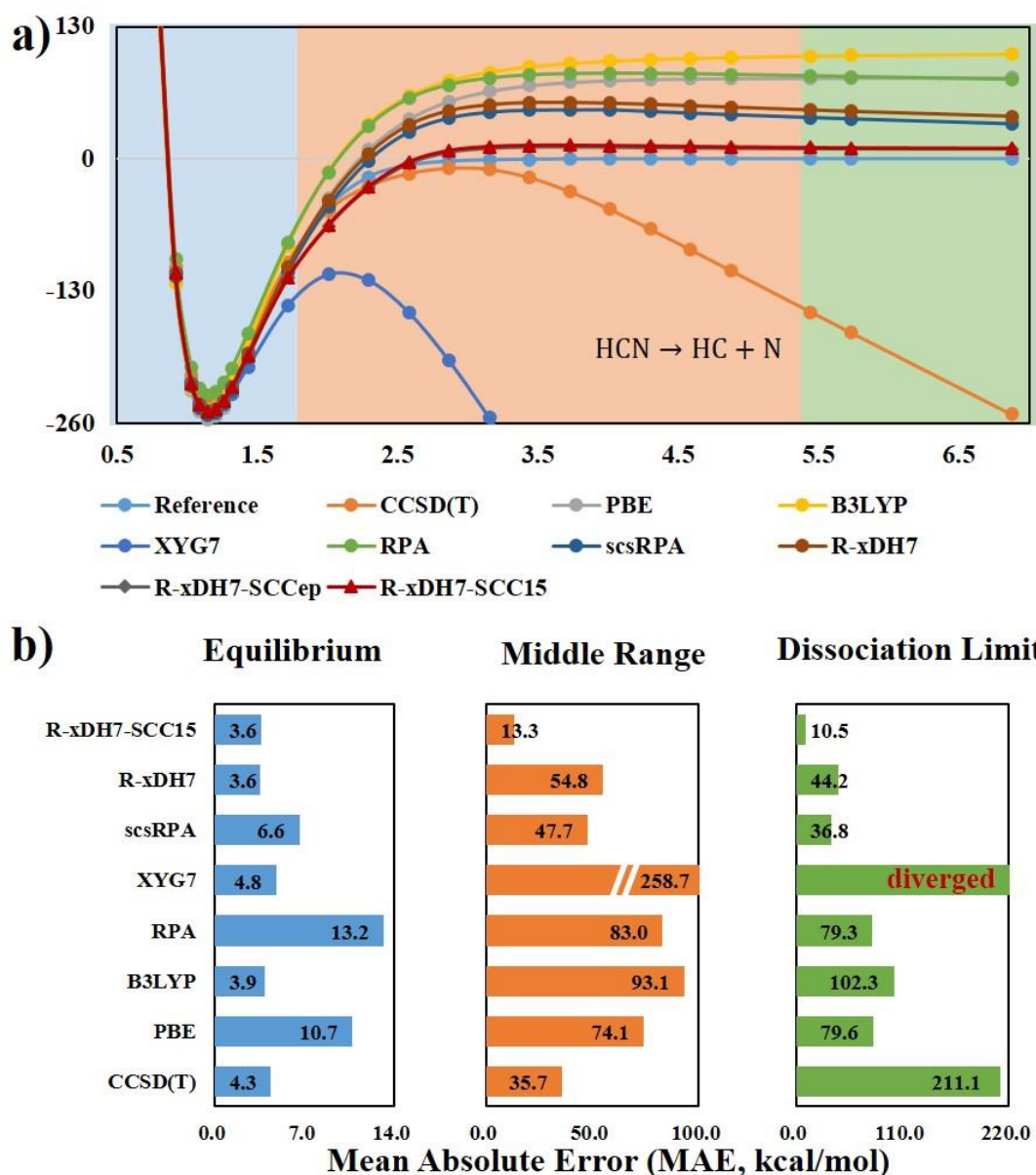
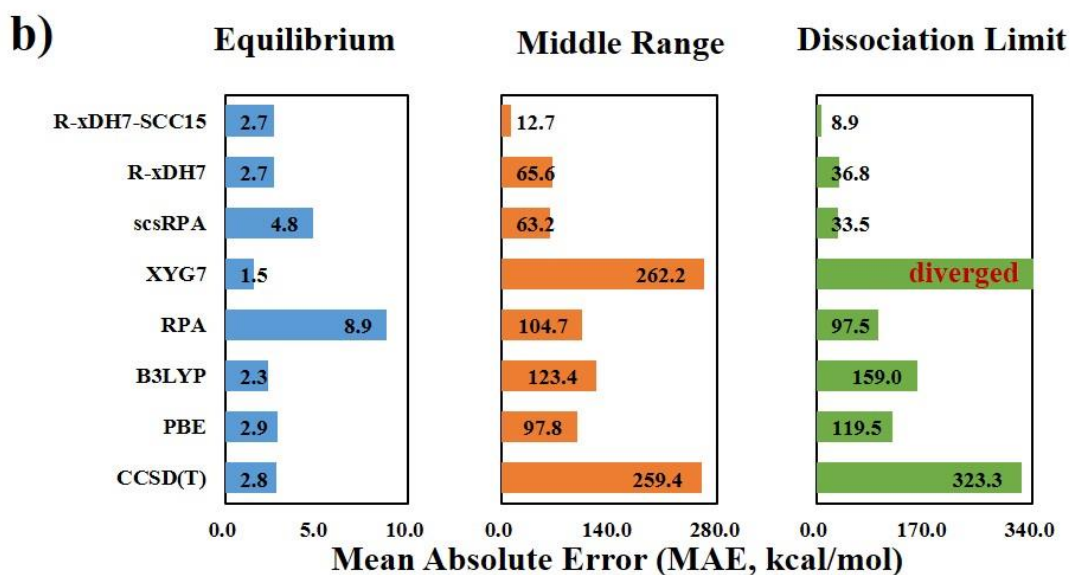
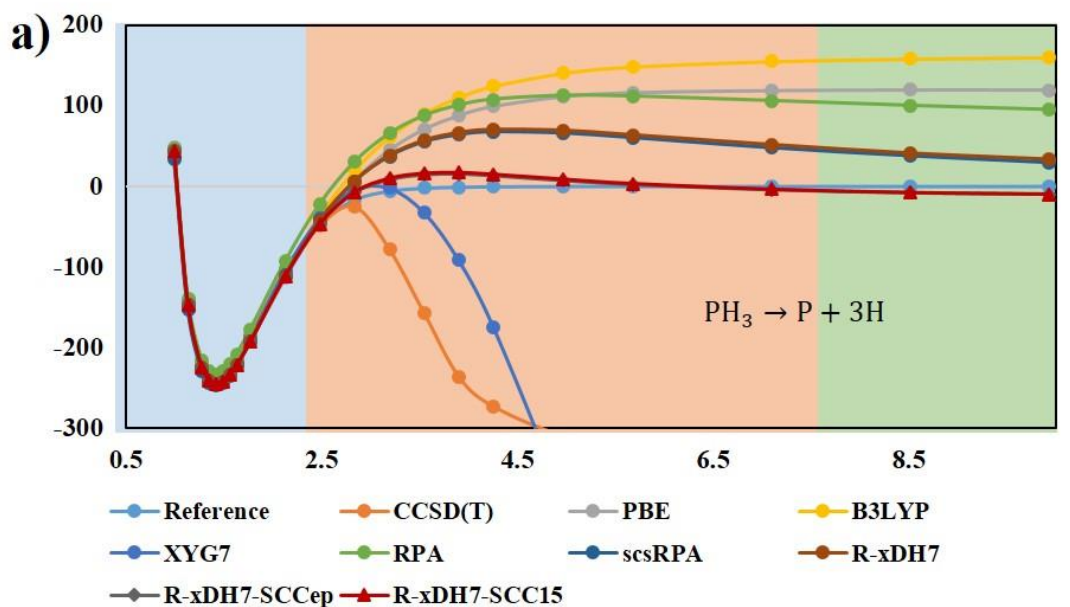


Figure S17 Performances of various methods on the (M5) HCN \rightarrow HC + N dissociation curve. a) Calculated potential energy curves for breaking C-N bond of the HCN molecule. b) Mean absolute errors (MAEs) of these methods in the regions of equilibrium, middle range, and dissociation limit of HCN \rightarrow HC + N dissociation curve.



*Unable to calculate the correct CCSD(T) results for bond length larger than 6.0Å.

Figure S18 | Performances of various methods on the (M6) PH₃ → P + 3H dissociation curve. a) Calculated potential energy curves for breaking three P-H bond of the PH₃ molecule. b) Mean absolute errors (MAEs) of these methods in the regions of equilibrium, middle range, and dissociation limit of PH₃ → P + 3H dissociation curve.

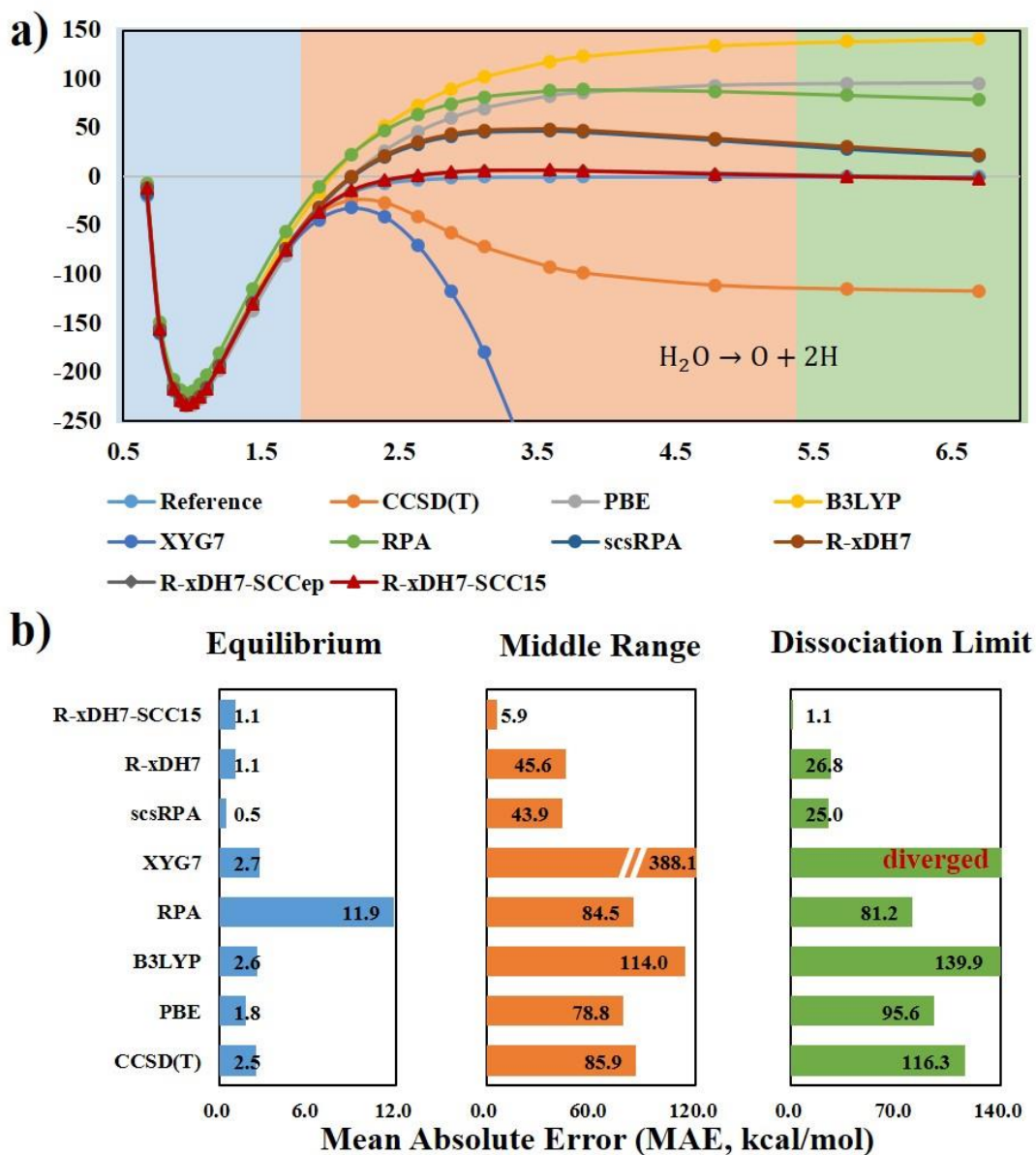


Figure S19 | Performances of various methods on the (M7) $\text{H}_2\text{O} \rightarrow \text{O} + 2\text{H}$ dissociation curve. a) Calculated potential energy curves for breaking two O-H bonds of the H_2O molecule. b) Mean absolute errors (MAEs) of these methods in the regions of equilibrium, middle range, and dissociation limit of $\text{H}_2\text{O} \rightarrow \text{O} + 2\text{H}$ dissociation curve.

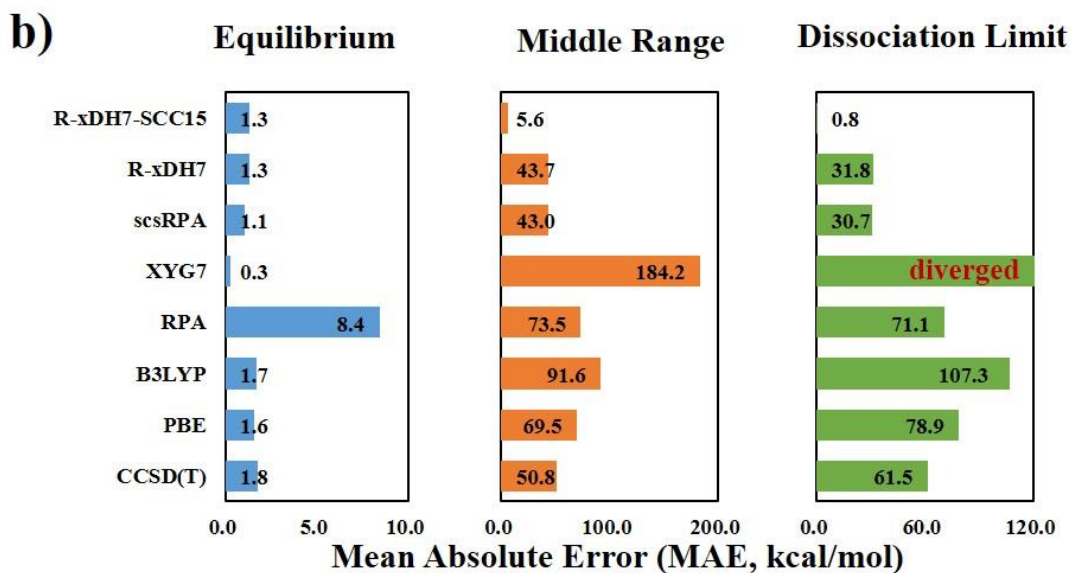
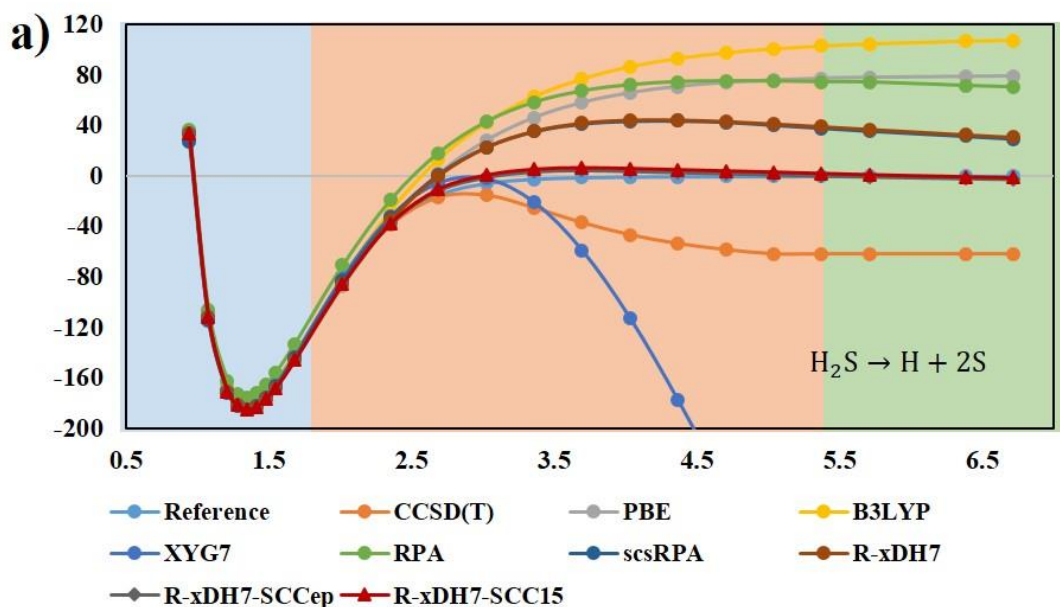
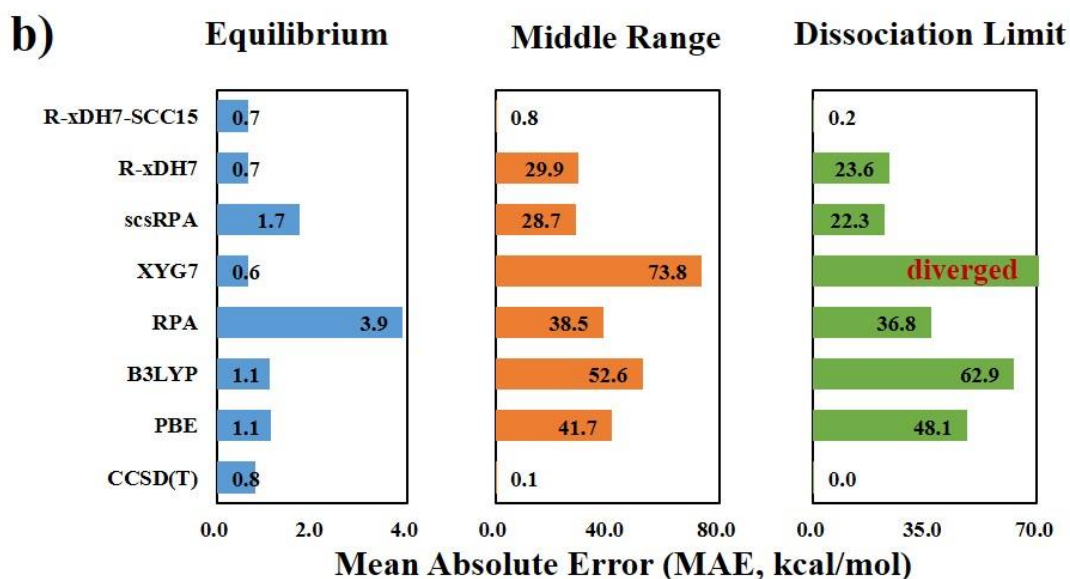
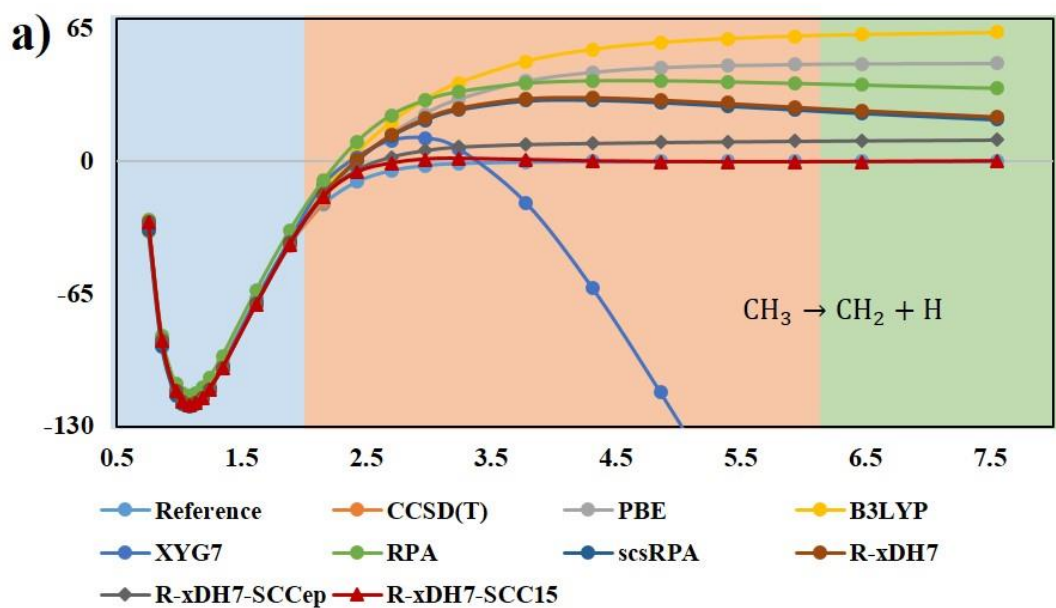
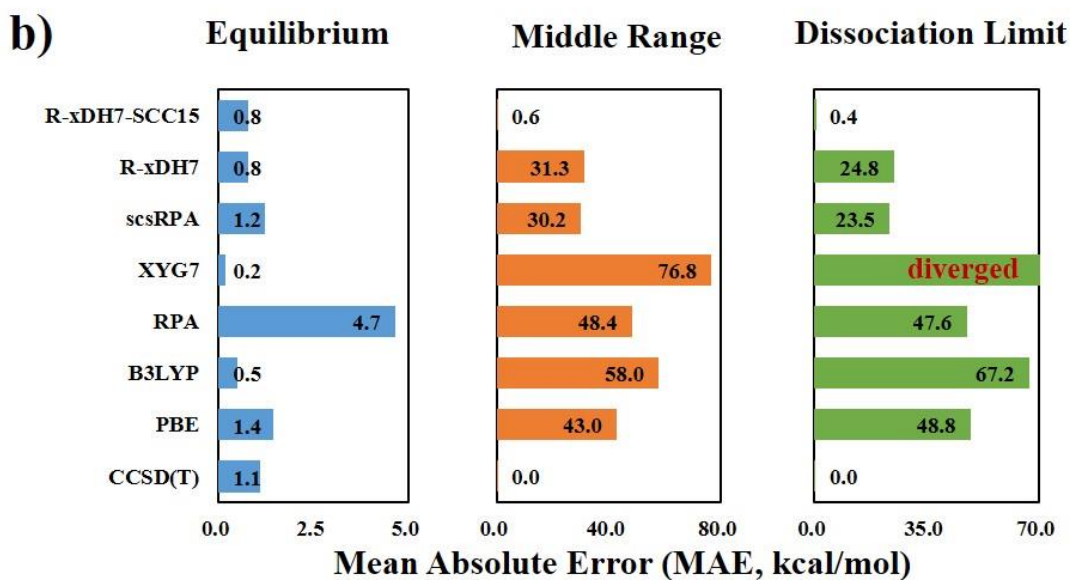
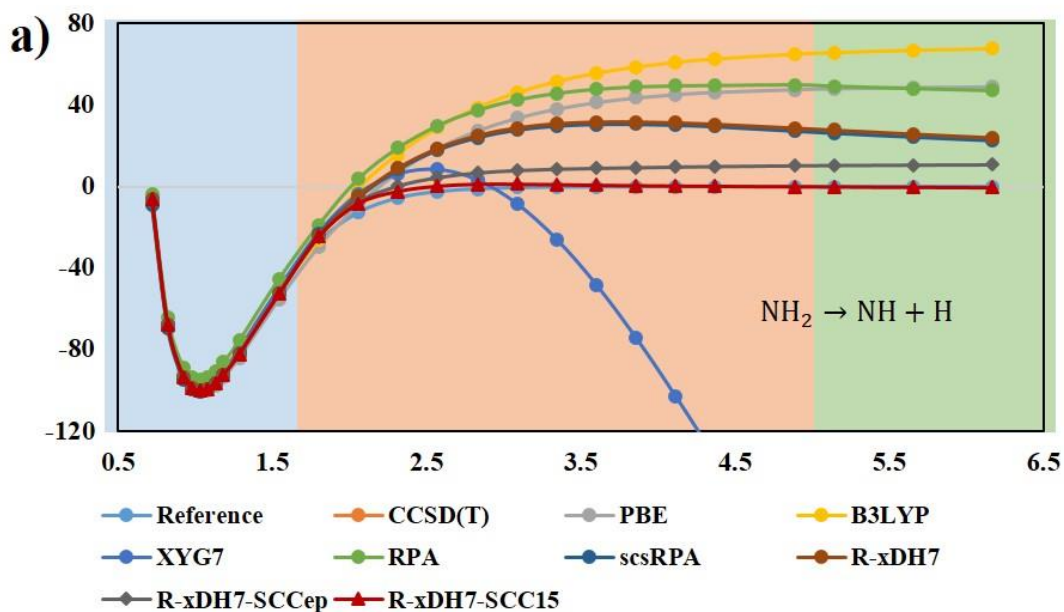


Figure S20 | Performances of various methods on the (M8) $\text{H}_2\text{S} \rightarrow \text{S} + 2\text{H}$ dissociation curve. a) Calculated potential energy curves for breaking two S-H bond of the H_2S molecule. b) Mean absolute errors (MAEs) of these methods in the regions of equilibrium, middle range, and dissociation limit of $\text{H}_2\text{S} \rightarrow \text{S} + 2\text{H}$ dissociation curve.



*Unable to calculate the correct CCSD(T) results for bond length larger than 2.2Å.

Figure S21 | Performances of various methods on the (O1) CH₃ → CH₂ + H dissociation curve. a) Calculated potential energy curves for breaking C-H bond of the CH₃ radical. b) Mean absolute errors (MAEs) of these methods in the regions of equilibrium, middle range, and dissociation limit of CH₃ → CH₂ + H dissociation curve.



*Unable to calculate the correct CCSD(T) results for bond length larger than 2.0Å.

Figure S22 | Performances of various methods on the (O2) $\text{NH}_2 \rightarrow \text{NH} + \text{H}$ dissociation curve. a) Calculated potential energy curves for breaking N-H bond of the NH_2 radical. b) Mean absolute errors (MAEs) of these methods in the regions of equilibrium, middle range, and dissociation limit of $\text{NH}_2 \rightarrow \text{NH} + \text{H}$ dissociation curve.

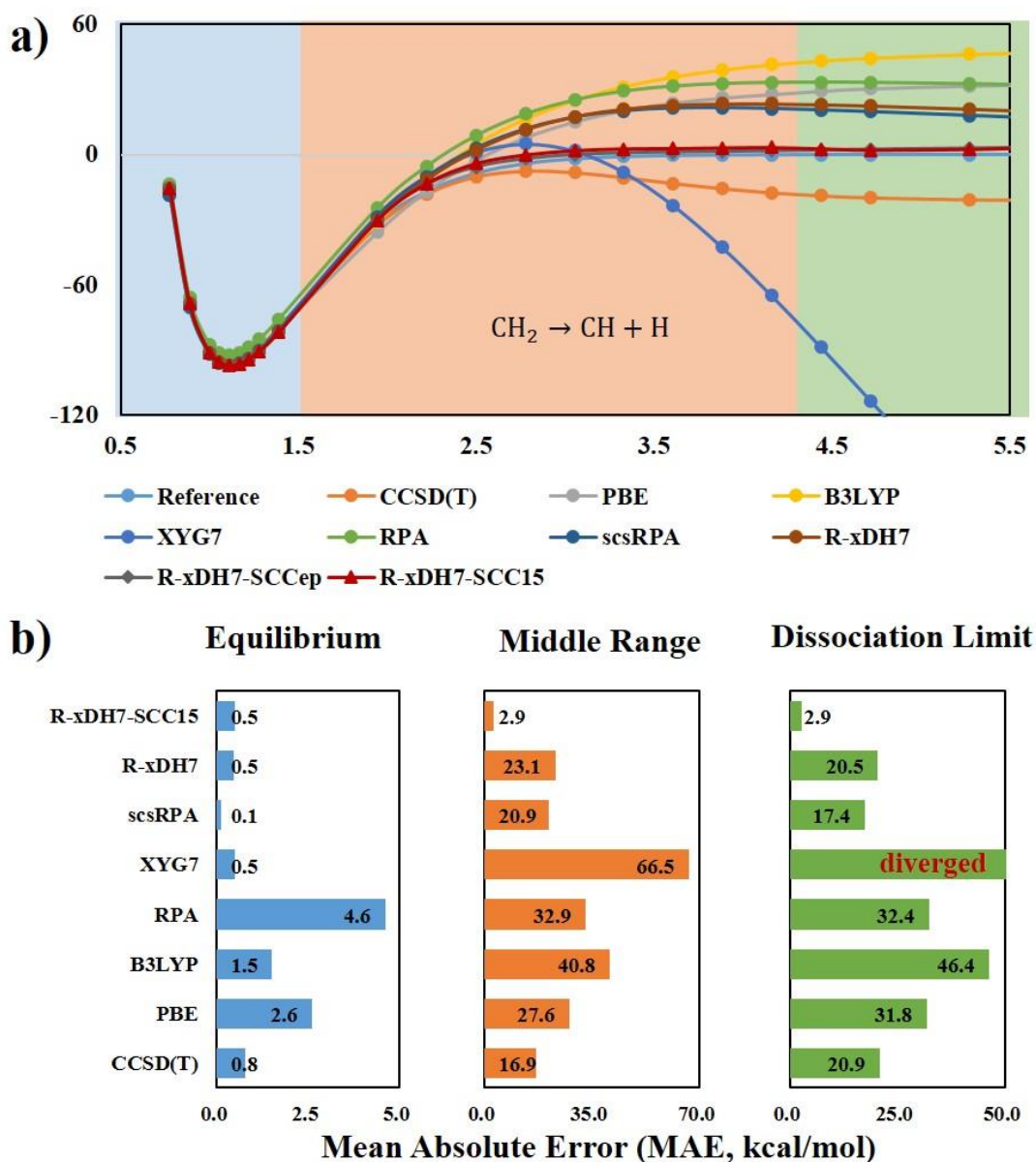


Figure S23 | Performances of various methods on the (O3) $\text{CH}_2 \rightarrow \text{CH} + \text{H}$ dissociation curve. a) Calculated potential energy curves for breaking C-H bond of the CH_2 molecule. b) Mean absolute errors (MAEs) of these methods in the regions of equilibrium, middle range, and dissociation limit of $\text{CH}_2 \rightarrow \text{CH} + \text{H}$ dissociation curve.

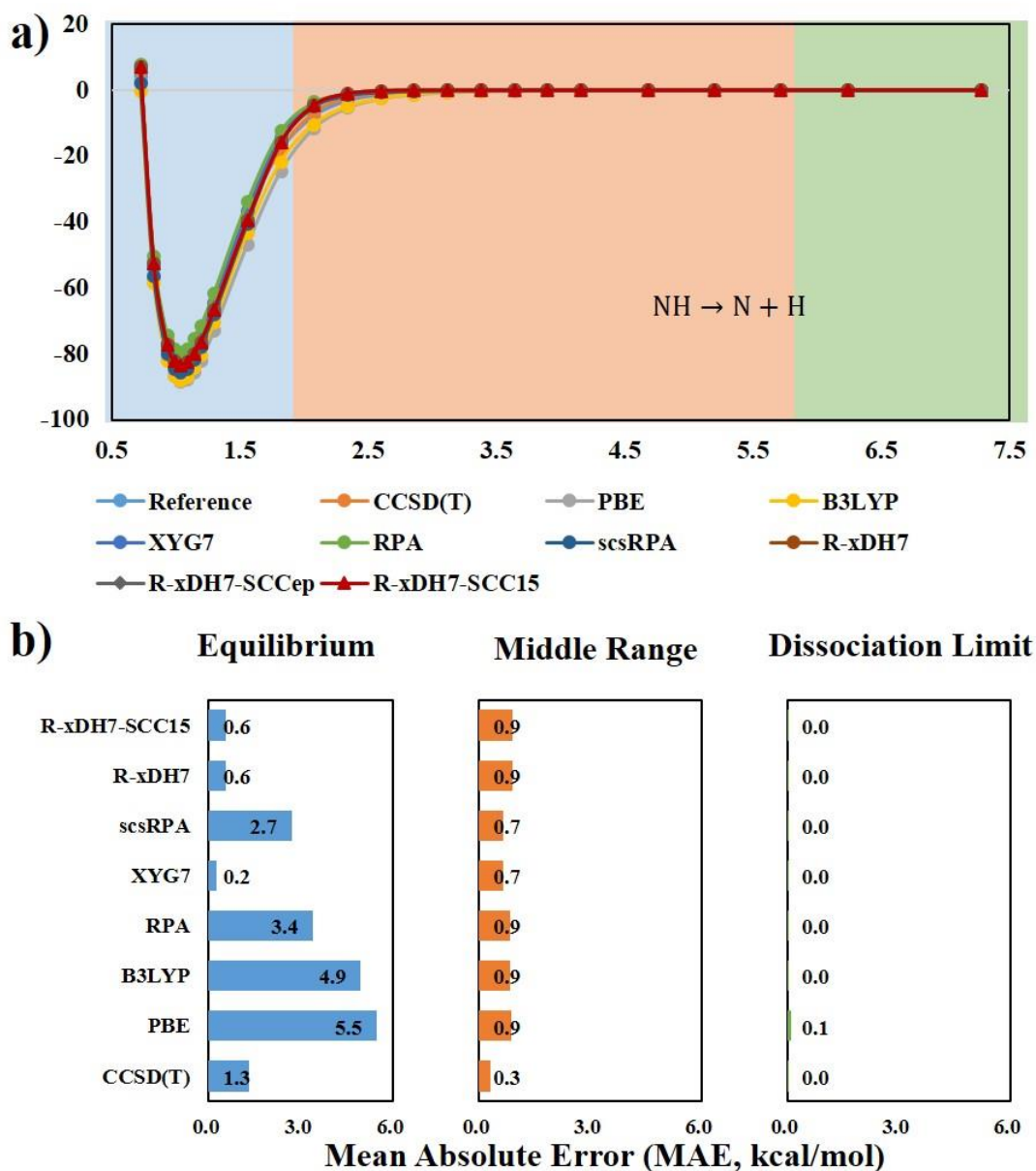
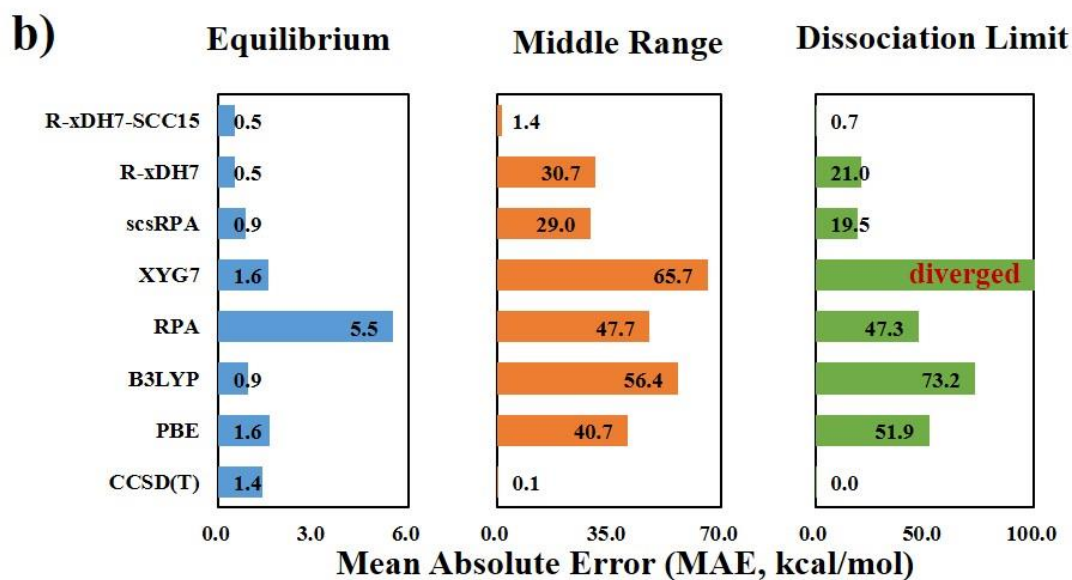
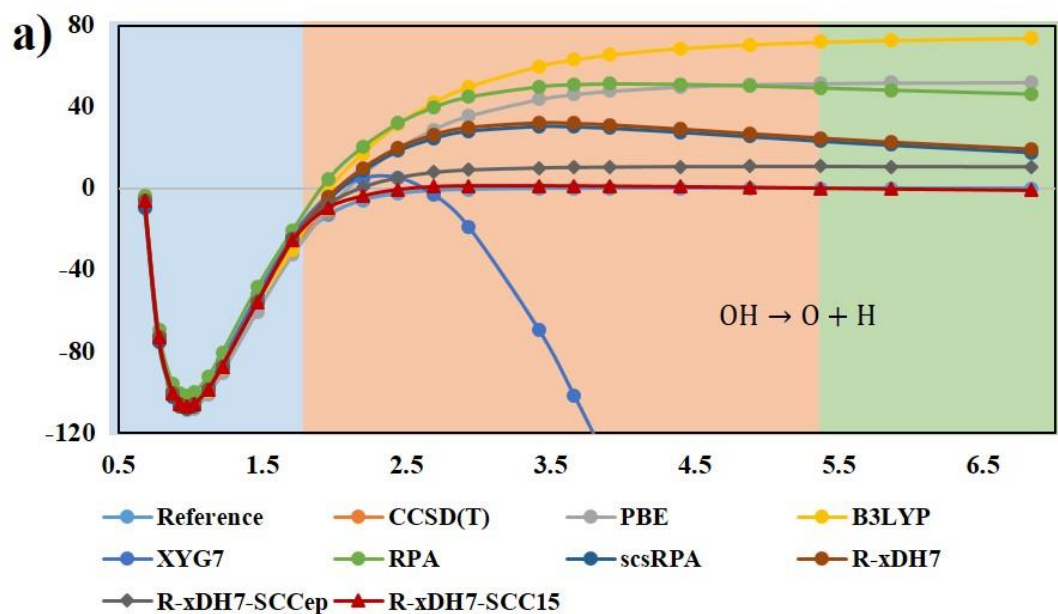
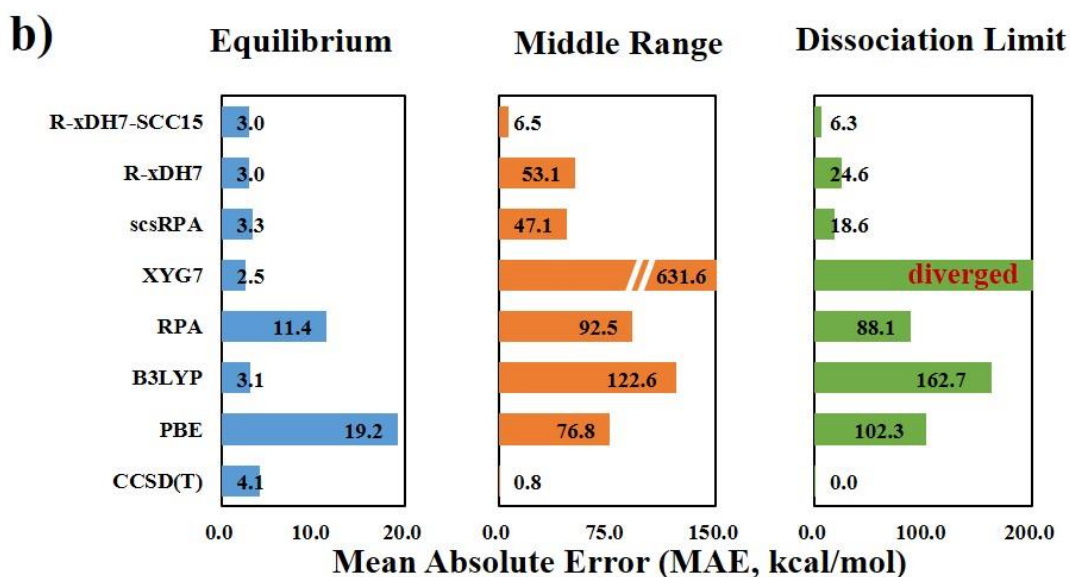
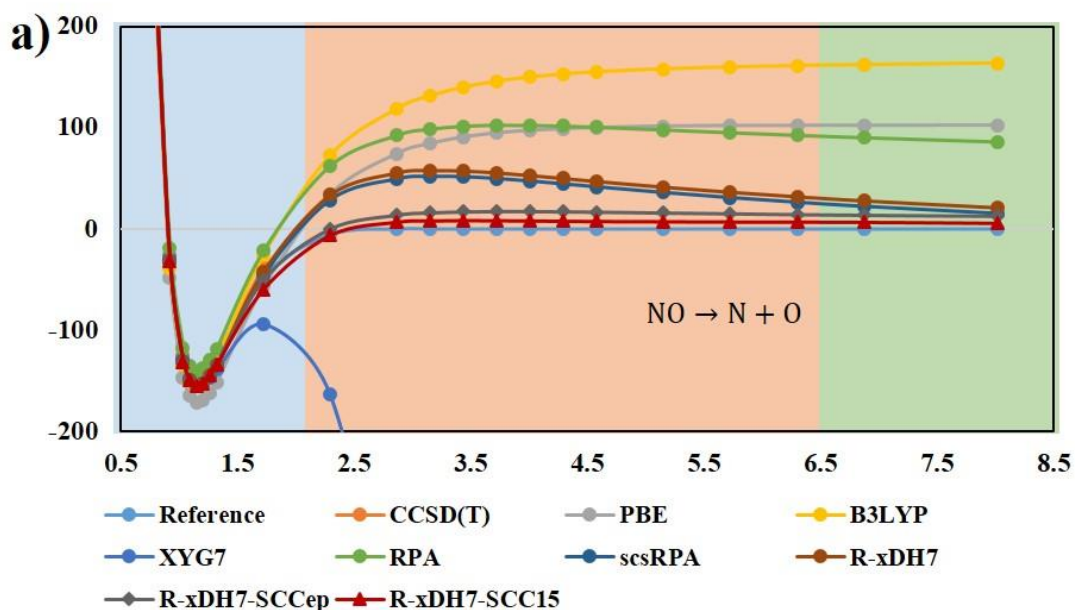


Figure S24 Performances of various methods on the (O4) $\text{NH} \rightarrow \text{N} + \text{H}$ dissociation curve. a) Calculated potential energy curves for breaking N-H bond of the NH radical. b) Mean absolute errors (MAEs) of these methods in the regions of equilibrium, middle range, and dissociation limit of $\text{NH} \rightarrow \text{N} + \text{H}$ dissociation curve.



*Unable to calculate the correct CCSD(T) results for bond length larger than 2.0Å.

Figure S25 Performances of various methods on the (O5) OH → O + H dissociation curve. a) Calculated potential energy curves for breaking O-H bond of the OH radical. b) Mean absolute errors (MAEs) of these methods in the regions of equilibrium, middle range, and dissociation limit of OH → O + H dissociation curve.



*Unable to calculate the correct CCSD(T) results for bond length larger than 2.0Å.

Figure S26 Performances of various methods on the (O6) $\text{NO} \rightarrow \text{N} + \text{O}$ dissociation curve. a) Calculated potential energy curves for breaking N-O bond of the NO molecule. b) Mean absolute errors (MAEs) of these methods in the regions of equilibrium, middle range, and dissociation limit of $\text{NO} \rightarrow \text{N} + \text{O}$ dissociation curve.

5. Supplementary Tables

Table S1| Results of scsRPA, R-xDH7, R-xDH7-SCC15, B3LYP-D3BJ, PBE0-D3BJ, PBE-D3BJ, CCSD(T), XYG7 and RPA for MG23 in def2-QZVP (unit: kcal/mol). Reactions 18-21 were calculated with BSSE (Basis Set Superposition Error) correction. *Reference values of reactions 18-19 were calculated with i-FCIQMC with complete basis set extrapolated from def2-TZVP/def2-QZVP and BSSE correction, while that of reaction 20 was calculated with i-FCIQMC with def2-QZVP basis set and BSSE correction. **Reference value of reaction 15 was collected from ref. [1] using i-FCIQMC. (Please refer to Table S4 for more details.) Other reference values were collected from refs. [2, 3].

		ref	scsRPA	R-xDH7	R-xDH7-SCC15	B3LYP-D3BJ	PBE0-D3BJ	PBE-D3BJ	CCSD(T)	XYG7	RPA
1	NF ₃ → N + 3F	204.53	205.70	210.33	210.33	208.87	210.02	244.51	199.36	199.61	183.99
2	CO ₂ → C + 2O	389.61	386.54	391.25	391.25	389.27	392.16	416.59	383.08	389.18	366.63
3	SiO _{sin} → Si + O	192.40	190.72	190.79	190.81	189.54	183.44	196.76	187.95	193.39	178.63
4	SO ₂ → S + 2O	259.61	256.27	258.94	258.97	254.52	254.38	280.81	251.23	258.06	236.32
5	CO → C + O	259.42	258.22	260.52	260.52	256.10	255.74	269.14	255.66	259.37	245.38
6	SO _{tri} → Si + O	125.69	123.36	122.96	122.98	127.75	127.49	141.28	121.86	124.66	116.21
7	ClO → Cl + O	64.84	63.54	64.38	64.38	66.73	67.50	81.56	61.32	63.10	56.20
8	F ₂ → 2F	38.27	38.45	39.73	39.74	37.08	34.87	52.65	36.33	33.84	29.60
9	N ₂ → 2N	228.48	233.27	231.98	231.99	230.14	225.37	243.44	222.51	230.53	213.72
10	O ₂ → 2O	120.37	118.37	117.38	117.39	124.03	124.35	143.38	117.00	118.35	111.23
11	NO → N + O	152.70	155.35	155.07	155.07	155.64	153.30	172.12	147.99	153.31	140.59
12	CN → C + N	181.27	181.13	180.35	180.37	180.41	179.09	197.72	174.72	184.33	166.28
13	B ₂ → 2B	67.40	59.20	59.17	64.72	61.41	66.38	79.89	64.23	66.02	56.85
14	O ₃ → O ₂ + O	26.61	30.56	33.15	35.40	17.24	14.65	41.60	22.07	34.60	11.40
**15	C ₂ → 2C	145.22	138.48	138.57	141.49	120.66	120.89	154.87	142.91	157.40	120.27
16	S ₄ → 2S ₂	25.75	24.45	28.64	29.82	18.97	19.85	31.52	21.84	31.87	12.83
17	Cl ₂ O → Cl ₂ + O	41.71	42.69	43.17	43.16	42.25	40.68	54.21	39.46	40.40	34.83
*18	CaO → Ca + O	83.57	85.69	85.00	83.47	105.60	102.29	123.79	79.22	94.17	76.09
*19	LiO ⁻ → Li + O ⁻	58.69	56.61	57.87	58.96	54.11	53.28	70.48	61.83	78.79	46.92
*20	KO ⁻ → K + O ⁻	41.14	35.71	36.13	42.63	27.45	25.56	50.76	38.44	80.38	23.81
21	MgS → Mg + S	55.68	47.42	49.11	47.88	49.61	50.40	56.75	49.40	52.25	41.87
22	O ₃ + C ₂ H ₂ → O ₃ -C ₂ H ₂ -add	-63.80	-62.71	-65.30	-63.81	-67.44	-74.69	-63.42	-64.74	-53.99	-66.90
23	O ₃ + C ₂ H ₄ → O ₃ -C ₂ H ₄ -add	-57.15	-56.23	-58.90	-57.40	-57.93	-65.41	-52.44	-58.40	-48.91	-60.47
MAD			2.82	2.96	2.43	5.58	6.61	15.04	4.03	6.23	13.03

Table S2| 17 chemical reactions with SCCep, SCCmb or SCC15 values exceeding 3.0 kcal/mol, filtered out from GMTKN55, MGCDB84 and MG23. *a.* taken from ref.^[2], *b.* taken from ref. ^[1], *c.* taken from ref.^[4], *d.* taken from ref. ^[5], while *e.* calculated with i-FCIQMC with def2-QZVP basis set and BSSE correction (see Table S4).

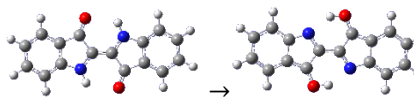
No.	Reaction name	Reaction	Reference (kcal/mol)
1	MG23-13	$B_2 \rightarrow 2B$	67.40 ^a
2	MG23-15	$C_2 \rightarrow 2C$	145.22 ^b
3	MG23-16	$S_4 \rightarrow 2S_2$	25.75 ^a
4	MG23-20	$KO^- \rightarrow K + O^-$	41.14 ^e
5	TAE140MR-5	$S_4 \rightarrow 4S$	234.30 ^c
6	ALKBDE10-8	$MgO \rightarrow Mg + O$	62.20 ^d
7	ALK8-1	$Li_8 \rightarrow 4Li_2$	81.75 ^e
8	ALK8-2	$Na_8 \rightarrow 4Na_2$	53.15 ^d
9	ALK8-6	$Li_5CH \rightarrow Li_4C + LiH$	66.28 ^d
10	ISOL24-11		36.90 ^d
11	BDE99MR-15	$S_4 \rightarrow S_3 + S$	65.98 ^c
12	HAT707MR-17	$HS + S_3 \rightarrow H + S_4$	21.75 ^c
13	HAT707MR-19	$BH + B \rightarrow H + B_2$	17.54 ^c
14	HAT707MR-43	$BN + B \rightarrow N + B_2$	38.36 ^c
15	HAT707MR-66	$SO + S_3 \rightarrow O + S_4$	60.48 ^c
16	HAT707MR-113	$BF + B \rightarrow F + B_2$	115.06 ^c
17	HAT707MR-124	$S_2 + S_3 \rightarrow S + S_4$	38.27 ^c

Table S3 | Results of scsRPA, R-xDH7, R-xDH7-SCC15, B3LYP-D3BJ, PBE0-D3BJ, PBE-D3BJ, CCSD(T), XYG7 and RPA for 17 chemical reactions with SCCep, SCCmb or SCC15 values exceeding 3.0 kcal/mol, filtered out from GMTKN55, MGCDB84 and MG23. *Reference values of reactions 4 and 7 were calculated using i-FCIQMC with def2-QZVP and BSSE correction.

No.	Reaction name	ref	scsRPA	R-xDH7	R-xDH7-SCCep	R-xDH7-SCC15	B3LYP-D3BJ	PBE0-D3BJ	PBE-D3BJ	CCSD(T)	XYG7	RPA
1	MG23-13	67.40	59.20	59.17	62.06	64.72	61.41	66.38	79.89	64.23	66.02	56.85
2	MG23-15	145.25	138.48	138.57	142.19	141.49	120.66	120.89	154.87	142.91	157.40	120.27
3	MG23-16	25.75	24.45	28.64	32.85	29.82	18.97	19.85	31.52	21.84	31.87	12.83
*4	MG23-20	41.14	35.71	36.13	53.18	42.63	27.45	25.56	50.76	38.44	80.38	23.81
5	TAE140MR-5	234.35	225.27	230.90	235.19	232.29	228.77	235.14	268.04	221.39	238.39	203.21
6	ALKBDE10-8	62.20	61.51	58.72	62.31	61.33	53.72	49.26	68.65	58.79	72.02	49.98
*7	ALK8-1	81.75	83.31	82.31	72.10	81.69	84.10	96.08	98.69	86.86	86.27	77.82
8	ALK8-2	53.15	67.73	51.06	43.72	51.74	48.45	60.52	60.02	67.66	60.16	66.44
9	ALK8-6	66.28	67.50	67.70	73.72	67.03	69.76	74.83	72.46	67.32	61.76	66.74
10	ISOL24-11	36.90	33.65	34.02	30.63	34.88	36.85	35.51	30.49	37.30	33.17	35.09
11	BDE99MR-15	65.98	62.18	63.84	66.88	64.50	63.98	66.61	76.20	61.92	69.15	55.86
12	HAT707MR-17	21.75	26.04	24.30	21.18	23.56	24.51	20.41	12.05	24.55	18.64	27.84
13	HAT707MR-19	17.54	26.29	25.81	22.59	19.81	23.18	14.47	4.05	19.93	18.13	23.94
14	HAT707MR-43	38.36	44.90	44.85	41.60	38.84	50.65	45.44	45.80	36.74	39.39	39.92
15	HAT707MR-66	60.48	61.38	59.15	56.11	58.49	62.85	60.83	65.26	59.96	55.73	60.64
16	HAT707MR-113	115.06	119.16	121.62	118.40	115.64	119.33	113.62	109.78	115.81	114.29	115.61
17	HAT707MR-124	38.27	38.23	37.31	34.27	36.65	40.59	41.17	39.85	37.89	34.18	39.42
MAD			4.73	3.82	4.87	1.73	6.31	6.41	9.80	3.65	6.48	9.10

Table S4 | Reactions with updated reference values calculated by i-FCIQMC. (unit: kcal/mol). Numbers in bold were chosen as the reference values in this work.

No.	Reaction name	Reaction		Original references		Updated references	Numerical uncertainty
1	MG23-15	$C_2 \rightarrow 2C$	146.88	QCISD/MG3 ^[2]	145.22	i-FCIQMC/VQZ+ $\Delta E_{F12}^{ccsd(T)}$ ^[1]	-
					83.31	i-FCIQMC/def2-QZVP(with BSSE)	± 0.63
					81.72	i-FCIQMC/cc-pVQZ (with BSSE)	± 1.88
						i-FCIQMC/CBS(def2-TZVP/def2-QZVP)	± 1.26
2	MG23-18	$CaO \rightarrow Ca + O$	96.15	ZPVE corrected experimental reference ^[27, 28]	86.00	(no BSSE)	
						i-FCIQMC/CBS(def2-TZVP/def2-QZVP)	± 1.26
					83.57	(with BSSE)	
						i-FCIQMC/def2-QZVP(with BSSE)	± 1.26
					57.79	i-FCIQMC/cc-pVQZ (with BSSE)	± 0.63
3	MG23-19	$LiO^- \rightarrow Li + O^-$	57.59	CCSDT(Q) ₂ /aug-cc-pCVQZ ^[29]	64.42	(no BSSE)	
						i-FCIQMC/CBS(def2-TZVP/def2-QZVP)	± 1.26
						(with BSSE)	
					58.69	(with BSSE)	
4	MG23-20	$KO^- \rightarrow K + O^-$	33.14	CCSD(T)/aug-cc-pCVQZ ^[29]	41.14	i-FCIQMC/def2-QZVP (with BSSE)	± 1.88
					81.75	i-FCIQMC/def2-QZVP (with BSSE)	± 0.19
					80.97	i-FCIQMC/cc-pVQZ (with BSSE)	± 0.06
						i-FCIQMC/CBS(cc-pVTZ/cc-pVQZ)	± 0.06
5	ALK8-1	$Li_8 \rightarrow 4Li_2$	86.47	CCSD(T)/CBS(aug-cc-pwCVTZ/aug-cc-pwCVQZ) ^[5]	80.41	(no BSSE)	
						i-FCIQMC/CBS(cc-pVTZ/cc-pVQZ)	± 0.06
					80.41	(with BSSE)	
						i-FCIQMC/def2-QZVP	± 1.26
6	G2RC-25	$Li_2 + F_2 \rightarrow 2LiF$	-211.7	ZPVE corrected experimental reference ^[30]	-212.73	i-FCIQMC/CBS(def2-TZVP/def2-QZVP)	± 1.26
			-216.11	W2-F12 ^[5]	-211.06	i-FCIQMC/CBS(cc-pVTZ/cc-pVQZ)	± 1.26

Table S5| Results of R-xDH7-SCC15, R-xDH7, B3LYP, PBE0, scsRPA, PBE, HF, XYG7, RPA and CISD at the thermodynamic limit (TDL) for hydrogen chains, calculated with def2-QZVPPD. The reference values were obtained from Ref.^[6]. (unit: kcal/mol). Hydrogen chains with nearest-neighbour proton separation (bond length) R of 1.4, 1.6, 1.8, 2.0, 2.4, 2.8, 3.2, 3.6 bohr are studied. According to the classification used in this work, all these bond lengths are within the equilibrium region. It is difficult to obtain the self-consistent converged TDL results in the outer regions.

d(Bohr)	AFQMC+ Δ DMRG (Reference)	R-xDH7-SCC1 5	R-xDH 7	B3LYP	PBE0	scsRPA	PBE	HF	XYG7	RPA	CISD
1.4	-25.24	-24.09	-24.07	-28.02	-25.63	-25.92	-27.40	-7.59	-24.15	-22.80	-19.65
1.6	-37.39	-36.42	-36.38	-39.86	-37.50	-37.57	-39.30	-19.43	-36.35	-34.68	-31.33
1.8	-41.18	-40.58	-40.52	-43.68	-41.29	-41.18	-43.40	-23.10	-40.37	-38.29	-34.56
2.0	-40.48	-40.17	-40.07	-42.97	-40.53	-40.34	-42.96	-22.16	-39.78	-37.40	-33.25
2.4	-33.20	-33.17	-32.95	-35.49	-32.85	-32.70	-35.92	-14.00	-32.36	-29.58	-24.52
2.8	-24.28	-23.65	-23.29	-25.44	-22.55	-22.78	-26.28	-3.10	-22.38	-19.34	-13.22
3.2	-16.00	-14.36	-13.89	-15.55	-12.36	-13.32	-16.76	7.82	-12.68	-9.39	-2.03
3.6	-10.00	-6.20	-5.69	-6.72	-3.21	-5.16	-8.28	17.81	-4.35	-0.61	8.12
MAE		1.14	1.36	2.18	1.65	1.32	2.00	20.50	1.92	4.46	9.67

Table S6 Results of scsRPA, R-xDH7, R-xDH7-SCC15 for GMTKN55 (unit: kcal/mol). G21EA, G21IP, WATER27, RG18, IL16 and AHB21 were calculated with def2-QZVPPD, while other subsets were calculated with def2-QZVP.

No.	subset	scsRPA	R-xDH7	R-xDH7-SCC15	No.	subset	scsRPA	R-xDH7	R-xDH7-SCC15
1	W4-11	3.34	2.01	1.94	36	ADIM6	0.52	0.31	0.31
2	G21EA	2.90	1.95	1.94	37	S22	0.19	0.19	0.19
3	G21IP	4.89	2.04	2.09	38	S66	0.24	0.16	0.16
4	DIPCS10	9.86	1.81	1.96	39	HEAVY28	0.33	0.10	0.10
5	PA26	4.67	0.96	0.98	40	WATER27	3.22	1.31	1.31
6	SIE4x4	10.21	5.65	5.87	41	CARBHB12	0.63	0.18	0.18
7	ALKBDE10	3.81	5.06	5.27	42	PNICO23	0.86	0.20	0.21
8	YBDE18	1.42	1.23	1.25	43	HAL59	0.55	0.37	0.36
9	AL2x6	2.04	0.73	0.73	44	AHB21	0.51	0.32	0.31
10	HEAVYSB11	1.63	0.68	0.68	45	CHB6	1.42	1.17	1.17
11	NBPRC	1.51	1.01	1.01	46	IL16	0.11	0.46	0.46
12	ALK8	2.82	1.60	1.45	47	IDISP	1.37	0.94	0.92
13	RC21	1.29	0.65	0.66	48	ICONF	0.21	0.06	0.06
14	G2RC	2.20	2.03	2.06	49	ACONF	0.02	0.02	0.02
15	BH76RC	1.46	1.08	1.08	50	AMINO20x4	0.17	0.06	0.06
16	FH51	1.23	1.16	1.16	51	PCONF21	0.40	0.13	0.13
17	TAUT15	0.54	0.30	0.30	52	MCONF	0.22	0.14	0.14
18	DC13	4.25	3.76	4.20	53	SCONF	0.15	0.09	0.09
19	MB16-43	17.90	13.05	13.26	54	UPU23	0.32	0.38	0.38
20	DARC	0.87	2.35	2.32	55	BUT14DIOL	0.12	0.02	0.02
21	RSE43	0.38	0.37	0.37		MoM	1.92	1.28	1.29
22	BSR36	0.49	0.74	0.74		WTMAD-2	3.54	2.23	2.24
23	CDIE20	0.26	0.33	0.31					
24	ISO34	0.82	0.72	0.71					
25	ISOL24	1.08	1.18	1.14					
26	C60ISO	7.51	4.35	4.04					
27	PAre1	0.67	0.49	0.49					
28	BH76	1.35	1.06	1.06					
29	BHPERI	0.90	0.67	0.69					
30	BHDIV10	1.20	1.00	1.00					
31	INV24	0.69	0.59	0.80					
32	BHROT27	0.35	0.19	0.19					
33	PX13	0.79	2.46	2.46					
34	WCPT18	0.51	1.69	1.77					
35	RG18	0.11	0.08	0.08					

Table S7 | MAD of scsRPA, R-xDH7, R-xDH7-SCC15, XYG7, XYG3, XYGJOS, ω B97M-V, CF22D, ω B97X-V, M06-2X-D3(0), MN15-D3(BJ), B3LYP-D3(BJ), M06-D3(0), PBE0-D3(BJ) and PBE-D3(BJ) for each subset of MGCDB84 using def2-QZVPPD (unit: kcal/mol).

Subset	Category	scsRPA	R-xDH7	R-xDH7-SCC15	XYG7
AlkAtom19	TCE	4.96	2.48	2.47	1.92
AlkIsod14	TCE	0.64	0.68	0.68	0.58
BDE99nonMR	TCE	1.47	1.43	1.43	1.16
BH76RC	TCE	1.14	0.91	0.91	0.94
BSR36	TCE	0.26	0.82	0.82	0.76
EA13	TCE	2.87	1.81	1.81	1.27
G21EA	TCE	2.71	1.86	1.86	1.23
G21IP	TCE	4.46	1.96	2.00	1.75
HAT707nonMR	TCE	1.92	1.88	1.89	1.46
HNBrBDE18	TCE	0.85	1.47	1.47	0.56
IP13	TCE	3.88	1.68	1.68	1.32
NBPRC	TCE	0.91	1.24	1.24	0.88
SN13	TCE	1.44	0.82	0.82	1.81
TAE140nonMR	TCE	3.17	1.82	1.83	2.15
WCPT6	TCE	0.49	0.25	0.26	0.72
BDE99MR	TCD	2.13	2.56	2.82	2.89
HAT707MR	TCD	2.37	2.43	2.43	2.06
PlatonicHD6	TCD	2.70	1.31	1.31	3.56
PlatonicID6	TCD	1.10	3.67	3.67	4.90
PlatonicIG6	TCD	6.04	2.23	2.23	10.35
PlatonicTAE6	TCD	19.02	1.34	1.34	6.11
TAE140MR	TCD	3.46	3.04	2.35	4.48
3B-69-DIM	NCED	0.22	0.14	0.14	0.09
A21x12	NCED	0.05	0.05	0.05	0.04
A24	NCED	0.13	0.10	0.10	0.10
AlkBind12	NCED	0.44	0.22	0.20	0.14
BzDC215	NCED	0.31	0.34	0.34	0.24
CO2Nitrogen16	NCED	0.38	0.14	0.14	0.09
DS14	NCED	0.27	0.07	0.07	0.11
HB15	NCED	0.12	0.15	0.15	0.25
HB49	NCED	0.26	0.14	0.14	0.22
HSG	NCED	0.27	0.16	0.16	0.06
HW30	NCED	0.06	0.20	0.20	0.19
Ionic43	NCED	3.15	0.46	0.46	1.54
NBC10	NCED	0.59	0.25	0.24	0.06
NC15	NCED	0.08	0.08	0.08	0.09
S22	NCED	0.50	0.27	0.27	0.17
S66	NCED	0.39	0.22	0.22	0.12
S66x8	NCED	0.28	0.18	0.18	0.09
X40	NCED	0.33	0.14	0.13	0.15

3B-69-TRIM	NCEC	0.67	0.41	0.40	0.23
CE20	NCEC	1.42	0.67	0.67	1.14
FmH2O10	NCEC	4.44	0.86	0.86	1.78
H2O20Bind10	NCEC	9.22	0.74	0.73	4.69
H2O20Bind4	NCEC	7.57	5.70	5.70	8.54
H2O6Bind8	NCEC	2.08	0.59	0.59	1.79
HW6Cl	NCEC	1.32	0.18	0.18	0.70
HW6F	NCEC	1.35	0.37	0.37	0.36
Shields38	NCEC	2.08	1.36	1.36	2.30
SW49Bind345	NCEC	0.54	0.18	0.18	0.14
SW49Bind6	NCEC	1.47	0.21	0.21	0.20
WATER27	NCEC	1.33	1.16	1.16	1.40
Bauza30	NCD	0.71	0.55	0.56	0.69
CT20	NCD	0.12	0.12	0.12	0.18
TA13	NCD	1.17	0.93	0.93	0.78
XB18	NCD	0.87	0.50	0.51	0.07
XB51	NCD	0.76	0.39	0.42	0.16
ACONF	IE	0.11	0.02	0.02	0.08
AlkIsomer11	IE	0.13	0.06	0.06	0.07
Butanediol65	IE	0.16	0.05	0.05	0.04
CYCONF	IE	0.17	0.08	0.08	0.06
H2O16Rel5	IE	0.28	0.35	0.35	0.29
H2O20Rel10	IE	0.13	0.09	0.09	0.11
H2O20Rel4	IE	0.36	0.36	0.36	0.28
Melatonin52	IE	0.40	0.13	0.13	0.12
Pentane14	IE	0.11	0.02	0.02	0.18
SW49Rel345	IE	0.08	0.17	0.17	0.14
SW49Rel6	IE	0.08	0.18	0.18	0.16
YMPJ519	IE	0.35	0.11	0.11	0.10
C20C24	ID	5.41	5.32	5.41	6.32
DIE60	ID	0.43	0.41	0.40	0.16
EIE22	ID	0.30	0.23	0.22	0.22
ISOMERIZATION20	ID	0.88	0.78	0.76	1.25
Styrene45	ID	1.89	2.12	2.13	0.96
BHPERI26	BH	0.64	0.66	0.69	0.62
CR20	BH	0.64	1.10	1.09	3.23
CRBH20	BH	2.56	0.34	0.34	4.27
DBH24	BH	1.06	0.88	0.88	0.93
HTBH38	BH	0.96	0.75	0.75	0.68
NHTBH38	BH	1.08	0.76	0.76	0.89
PX13	BH	0.92	3.07	3.07	2.48
RG10	BH	0.05	0.05	0.05	0.07
WCPT27	BH	0.48	1.90	1.95	1.48
MUE		0.90	0.67	0.67	0.65

Subset	Category	XYG3	XYGJOS	ωB97M-V	CF22D
AlkAtom19	TCE	2.01	7.38	0.87	0.61
AlkIsod14	TCE	1.57	2.13	0.97	0.51
BDE99nonMR	TCE	1.78	1.29	1.53	1.71
BH76RC	TCE	1.00	0.76	0.96	1.15
BSR36	TCE	2.54	3.91	0.99	0.50
EA13	TCE	1.98	1.74	1.77	1.80
G21EA	TCE	1.97	1.96	2.26	1.88
G21IP	TCE	1.37	1.42	2.86	2.78
HAT707nonMR	TCE	1.78	1.90	1.90	1.92
HNBBrBDE18	TCE	2.45	0.76	2.49	1.75
IP13	TCE	1.23	1.62	2.57	2.00
NBPRC	TCE	1.14	1.22	0.87	1.26
SN13	TCE	1.36	0.90	0.50	0.65
TAE140nonMR	TCE	2.07	2.43	1.59	1.73
WCPT6	TCE	0.88	0.62	0.34	0.57
BDE99MR	TCD	3.16	3.05	3.70	3.44
HAT707MR	TCD	2.11	2.46	3.31	3.37
PlatonicHD6	TCD	1.04	0.86	4.29	3.19
PlatonicID6	TCD	6.14	9.02	1.78	3.51
PlatonicIG6	TCD	22.83	18.71	4.77	3.76
PlatonicTAE6	TCD	6.09	5.66	4.02	3.50
TAE140MR	TCD	4.97	3.19	3.59	2.98
3B-69-DIM	NCED	0.31	0.37	0.12	0.31
A21x12	NCED	0.07	0.06	0.03	0.05
A24	NCED	0.19	0.15	0.07	0.13
AlkBind12	NCED	0.97	1.05	0.12	0.17
BzDC215	NCED	0.14	0.14	0.14	0.16
CO2Nitrogen16	NCED	0.46	0.62	0.07	0.49
DS14	NCED	0.26	0.27	0.13	0.18
HB15	NCED	0.32	0.25	0.17	0.38
HB49	NCED	0.22	0.24	0.18	0.30
HSG	NCED	0.48	0.50	0.09	0.15
HW30	NCED	0.09	0.06	0.13	0.20
Ionic43	NCED	1.47	1.50	0.51	0.50
NBC10	NCED	0.58	0.69	0.10	0.37
NC15	NCED	0.05	0.07	0.04	0.06
S22	NCED	0.50	0.68	0.21	0.54
S66	NCED	0.51	0.59	0.12	0.29
S66x8	NCED	0.40	0.46	0.07	0.20
X40	NCED	0.34	0.38	0.18	0.27
3B-69-TRIM	NCEC	0.79	1.04	0.27	0.88
CE20	NCEC	0.64	0.92	0.42	0.47
FmH2O10	NCEC	1.05	1.96	0.42	2.13
H2O20Bind10	NCEC	3.40	4.83	0.96	3.78

H2O20Bind4	NCEC	1.51	5.00	1.05	1.41
H2O6Bind8	NCEC	1.74	2.05	0.29	0.19
HW6Cl	NCEC	0.26	0.38	0.18	0.71
HW6F	NCEC	0.20	0.71	0.12	1.12
Shields38	NCEC	0.97	1.80	0.40	0.59
SW49Bind345	NCEC	0.46	0.26	0.22	0.22
SW49Bind6	NCEC	1.08	0.58	0.59	0.63
WATER27	NCEC	0.94	1.22	0.43	0.84
Bauza30	NCD	0.69	0.49	0.45	0.44
CT20	NCD	0.08	0.08	0.07	0.11
TA13	NCD	0.57	0.65	1.67	1.63
XB18	NCD	0.17	0.36	0.40	0.29
XB51	NCD	0.30	0.37	0.46	0.34
ACONF	IE	0.26	0.25	0.06	0.04
AlkIsomer11	IE	0.57	0.78	0.17	0.07
Butanediol65	IE	0.09	0.09	0.03	0.25
CYCONF	IE	0.19	0.10	0.06	0.19
H2O16Rel5	IE	0.61	0.67	0.03	0.04
H2O20Rel10	IE	0.24	0.25	0.09	0.15
H2O20Rel4	IE	0.72	0.78	0.11	0.21
Melatonin52	IE	0.39	0.55	0.13	0.30
Pentane14	IE	0.25	0.19	0.10	0.09
SW49Rel345	IE	0.09	0.14	0.12	0.10
SW49Rel6	IE	0.10	0.17	0.13	0.10
YMPJ519	IE	0.23	0.24	0.25	0.28
C20C24	ID	14.40	7.53	5.11	11.68
DIE60	ID	0.48	0.16	0.58	0.63
EIE22	ID	0.67	0.27	0.19	0.53
ISOMERIZATION20	ID	1.75	1.04	1.52	1.29
Styrene45	ID	2.54	1.05	1.48	1.21
BHPERI26	BH	0.58	2.34	1.15	1.12
CR20	BH	6.25	4.14	0.44	0.60
CRBH20	BH	5.59	2.89	1.06	2.17
DBH24	BH	0.84	0.80	1.10	1.37
HTBH38	BH	0.70	0.86	1.43	1.31
NHTBH38	BH	0.89	0.74	1.32	1.75
PX13	BH	1.05	2.40	2.08	1.17
RG10	BH	0.07	0.08	0.04	0.04
WCPT27	BH	0.60	0.80	1.36	1.21
MUE		0.85	0.89	0.70	0.78

Subset	Category	ω B97X-V	M06-2X-D3(0)	MN15-D3(BJ)	B3LYP-D3(BJ)
AlkAtom19	TCE	1.62	7.42	0.31	1.26
AlkIsod14	TCE	1.68	1.33	0.88	2.08
BDE99nonMR	TCE	2.25	1.83	0.09	2.77
BH76RC	TCE	1.54	0.86	0.20	2.03
BSR36	TCE	2.55	3.03	0.52	3.90
EA13	TCE	2.43	2.08	13.97	2.27
G21EA	TCE	2.58	2.42	1.07	2.29
G21IP	TCE	2.96	2.54	1.10	3.71
HAT707nonMR	TCE	3.02	2.50	0.52	2.92
HNBBrBDE18	TCE	2.35	2.93	0.63	4.15
IP13	TCE	3.01	2.42	4.40	4.62
NBPRC	TCE	1.60	1.10	2.37	1.92
SN13	TCE	0.82	0.69	1.55	1.55
TAE140nonMR	TCE	2.20	2.10	1.26	3.04
WCPT6	TCE	0.88	0.80	0.48	0.99
BDE99MR	TCD	4.07	6.32	0.39	2.85
HAT707MR	TCD	3.96	5.08	0.42	3.02
PlatonicHD6	TCD	4.78	7.29	9.04	2.98
PlatonicID6	TCD	3.94	11.14	0.77	7.74
PlatonicIG6	TCD	5.49	8.70	0.30	19.77
PlatonicTAE6	TCD	7.27	10.58	1.44	14.32
TAE140MR	TCD	3.46	6.90	0.88	3.40
3B-69-DIM	NCED	0.14	0.22	0.15	0.22
A21x12	NCED	0.02	0.08	0.37	0.05
A24	NCED	0.05	0.16	1.32	0.12
AlkBind12	NCED	0.10	0.36	0.77	0.14
BzDC215	NCED	0.15	0.27	0.20	0.14
CO2Nitrogen16	NCED	0.09	0.12	1.50	0.06
DS14	NCED	0.09	0.15	0.71	0.19
HB15	NCED	0.22	0.28	3.49	0.60
HB49	NCED	0.20	0.30	1.56	0.42
HSG	NCED	0.12	0.17	2.78	0.14
HW30	NCED	0.11	0.28	0.89	0.18
Ionic43	NCED	0.61	0.79	6.41	0.64
NBC10	NCED	0.18	0.19	1.67	0.19
NC15	NCED	0.04	0.11	0.69	0.07
S22	NCED	0.20	0.33	0.80	0.30
S66	NCED	0.09	0.25	0.38	0.25
S66x8	NCED	0.12	0.20	4.71	0.18
X40	NCED	0.19	0.19	2.69	0.22
3B-69-TRIM	NCEC	0.31	0.49	0.49	0.59
CE20	NCEC	0.38	1.13	0.42	1.62
FmH2O10	NCEC	0.13	9.86	2.25	2.60
H2O20Bind10	NCEC	1.17	7.51	0.22	8.84

H2O20Bind4	NCEC	1.85	6.77	1.06	11.90
H2O6Bind8	NCEC	0.43	1.91	0.32	2.35
HW6Cl	NCEC	0.32	2.70	1.86	0.89
HW6F	NCEC	0.11	4.03	2.15	0.32
Shields38	NCEC	0.59	2.13	0.56	2.85
SW49Bind345	NCEC	0.25	0.59	2.62	0.68
SW49Bind6	NCEC	0.61	1.31	1.49	1.40
WATER27	NCEC	0.80	2.70	0.39	2.35
Bauza30	NCD	0.66	0.94	0.27	1.30
CT20	NCD	0.08	0.15	1.99	0.22
TA13	NCD	1.75	1.07	0.09	2.73
XB18	NCD	0.49	0.51	1.76	0.28
XB51	NCD	0.53	0.50	0.27	0.70
ACONF	IE	0.02	0.27	13.07	0.06
AlkIsomer11	IE	0.58	0.10	10.49	0.93
Butanediol65	IE	0.03	0.12	11.20	0.26
CYCONF	IE	0.08	0.18	9.77	0.26
H2O16Rel5	IE	0.30	1.37	2.57	0.64
H2O20Rel10	IE	0.07	0.79	0.04	0.23
H2O20Rel4	IE	0.22	1.38	0.57	0.66
Melatonin52	IE	0.10	0.33	0.53	0.27
Pentane14	IE	0.06	0.11	0.35	0.15
SW49Rel345	IE	0.19	0.14	0.53	0.48
SW49Rel6	IE	0.19	0.18	2.81	0.64
YMPJ519	IE	0.24	0.39	2.38	0.37
C20C24	ID	4.31	19.30	0.16	27.20
DIE60	ID	0.65	0.57	0.40	1.13
EIE22	ID	0.22	0.32	0.14	1.35
ISOMERIZATION20	ID	1.27	1.13	0.25	1.79
Styrene45	ID	2.82	2.32	1.57	5.59
BHPERI26	BH	2.12	1.33	5.77	1.19
CR20	BH	2.82	1.67	2.30	6.38
CRBH20	BH	2.97	1.31	0.91	8.24
DBH24	BH	1.39	0.85	1.86	4.62
HTBH38	BH	2.04	1.09	1.19	5.18
NHTBH38	BH	1.38	1.29	0.27	4.93
PX13	BH	2.84	6.22	0.25	5.93
RG10	BH	0.04	0.07	0.42	0.04
WCPT27	BH	1.67	2.97	0.61	3.49
MUE		0.96	1.14	1.16	1.31

Subset	Category	M06-D3(0)	PBE0-D3(BJ)	PBE-D3(BJ)
AlkAtom19	TCE	3.18	8.34	22.24
AlkIsod14	TCE	0.98	2.21	2.01
BDE99nonMR	TCE	2.51	3.65	7.32
BH76RC	TCE	1.51	2.36	4.50
BSR36	TCE	1.60	3.82	3.72
EA13	TCE	2.88	2.73	2.50
G21EA	TCE	3.29	2.91	2.35
G21IP	TCE	3.12	3.60	3.79
HAT707nonMR	TCE	3.44	4.10	6.17
HNBBrBDE18	TCE	2.80	2.01	2.54
IP13	TCE	2.55	3.09	3.52
NBPRC	TCE	2.57	3.42	2.58
SN13	TCE	1.52	1.26	4.91
TAE140nonMR	TCE	2.58	3.37	14.32
WCPT6	TCE	1.15	0.96	1.04
BDE99MR	TCD	2.47	3.10	12.67
HAT707MR	TCD	3.47	3.30	7.35
PlatonicHD6	TCD	9.06	3.78	8.41
PlatonicID6	TCD	8.28	7.26	5.24
PlatonicIG6	TCD	20.61	11.37	4.69
PlatonicTAE6	TCD	9.92	43.38	75.85
TAE140MR	TCD	4.25	2.85	27.37
3B-69-DIM	NCED	0.29	0.29	0.30
A21x12	NCED	0.11	0.10	0.13
A24	NCED	0.16	0.20	0.31
AlkBind12	NCED	1.38	0.10	0.11
BzDC215	NCED	0.23	0.28	0.22
CO2Nitrogen16	NCED	0.62	0.28	0.39
DS14	NCED	0.17	0.28	0.40
HB15	NCED	0.32	0.89	0.80
HB49	NCED	0.34	0.61	0.88
HSG	NCED	0.33	0.14	0.21
HW30	NCED	0.28	0.25	0.29
Ionic43	NCED	0.48	0.94	0.95
NBC10	NCED	0.37	0.15	0.15
NC15	NCED	0.19	0.12	0.21
S22	NCED	0.30	0.45	0.43
S66	NCED	0.49	0.29	0.30
S66x8	NCED	0.37	0.27	0.28
X40	NCED	0.38	0.30	0.35
3B-69-TRIM	NCEC	0.70	0.71	0.71
CE20	NCEC	0.56	2.30	3.86
FmH2O10	NCEC	7.34	7.28	6.20
H2O20Bind10	NCEC	3.42	13.61	14.32

H2O20Bind4	NCEC	3.97	14.75	24.57
H2O6Bind8	NCEC	0.80	3.92	4.14
HW6Cl	NCEC	1.57	2.45	2.99
HW6F	NCEC	1.61	2.21	0.77
Shields38	NCEC	0.85	3.86	5.86
SW49Bind345	NCEC	0.85	0.77	1.39
SW49Bind6	NCEC	1.59	1.61	2.79
WATER27	NCEC	1.20	3.65	5.15
Bauza30	NCD	1.59	2.43	3.21
CT20	NCD	0.47	0.18	0.31
TA13	NCD	1.80	2.45	4.66
XB18	NCD	0.30	0.29	1.06
XB51	NCD	0.44	0.71	1.64
ACONF	IE	0.50	0.06	0.07
AlkIsomer11	IE	0.54	1.01	0.94
Butanediol65	IE	0.21	0.17	0.38
CYCONF	IE	0.12	0.56	0.82
H2O16Rel5	IE	3.37	1.25	1.46
H2O20Rel10	IE	1.44	0.41	0.46
H2O20Rel4	IE	3.61	1.44	1.66
Melatonin52	IE	0.49	0.32	0.52
Pentane14	IE	0.25	0.08	0.28
SW49Rel345	IE	0.53	0.52	0.88
SW49Rel6	IE	0.65	0.68	1.16
YMPJ519	IE	0.67	0.43	0.47
C20C24	ID	22.02	8.93	10.96
DIE60	ID	1.14	1.35	1.81
EIE22	ID	1.10	1.28	1.93
ISOMERIZATION20	ID	1.81	1.73	2.95
Styrene45	ID	3.72	3.02	2.46
BHPERI26	BH	1.92	3.23	6.65
CR20	BH	11.24	2.24	1.48
CRBH20	BH	8.73	1.10	7.76
DBH24	BH	1.97	3.72	8.41
HTBH38	BH	1.89	4.82	10.01
NHTBH38	BH	1.86	3.54	8.49
PX13	BH	1.38	8.53	15.28
RG10	BH	0.10	0.05	0.06
WCPT27	BH	1.66	5.57	10.82
MUE		1.32	1.52	1.72

Table S8 | Time consumption of various methods for several large species in GMTKN55 with def2-QZVP basis set. The calculations were paralleled with 36 cores of Intel® Xeon® Gold 6150 CPU @ 2.70GHz.

Subset	Species	Atom Number	Occupied Orbital Number	Virtual Orbital Number	Time per Iteration of B3LYP	Time for post SCF procedure of XYG7	Time for post SCF procedure of R-xDH7	Time for AI correction of R-xDH7-SCC15
ISOL24	i4e	81	119	3148	~560s	~233s	~293s	~312s
ISOL24	i4p	81	119	3148	~560s	~299s	~287s	~325s
IDISP	F22f	68	89	2545	~240s	~109s	~123s	~126s
IDISP	F22l	68	89	2545	~240s	~122s	~119s	~119s
WATER27	H2O20	60	100	2240	~150s	~102s	~94s	~123s
WATER27	H2O20es	60	100	2240	~143s	~101s	~92s	~128s
WATER27	H2O20fc	60	100	2240	~170s	~110s	~94s	~130s
WATER27	H2O20fs	60	100	2240	~165s	~96s	~96s	~121s

Table S9 | Active space selection of species in different dissociation curves and parameter settings of damping function for fitting reference values.

Dissociation curve	Species	Number of electrons in active space (α, β)	Number of orbitals in active space	A	$D_{eq}(\text{\AA})$	n
$H_2 \rightarrow 2H$	H_2	(1, 1)	2	1.75	0.75	4
	H	(1, 0)	1			
$C_2 \rightarrow 2C$	C_2	(4, 4)	8	1.30	1.25	8
	C	(3, 1)	4			
$N_2 \rightarrow 2N$	N_2	(3, 3)	6	1.25	1.10	8
	N	(3, 0)	3			
$F_2 \rightarrow 2F$	F_2	(1, 1)	2	1.25	1.40	8
	F	(1, 0)	1			
$C_2H_6 \rightarrow 2CH_3$	C_2H_6	(1, 1)	2	1.40	1.45	5
	CH_3	(1, 0)	1			
	H_2O	(4, 4)	6			
$H_2O \rightarrow O + 2H$	O	(4, 2)	4	1.40	0.96	8
	H	(1, 0)	1			
	CH_4	(4, 4)	8			
$CH_4 \rightarrow C + 4H$	C	(3, 1)	4	1.50	1.09	8
	H	(1, 0)	1			
	NH_3	(3, 3)	6			
$NH_3 \rightarrow N + 3H$	N	(3, 0)	3	1.50	1.01	13
	H	(1, 0)	1			
	HF	(1, 1)	2			
$HF \rightarrow H + F$	H	(1, 0)	1	1.40	0.93	10
	F	(1, 0)	1			
$H_2O \rightarrow OH + H$	H_2O	(1, 1)	2	1.50	0.96	10
	OH	(1, 0)	1			
	H	(1, 0)	1			
$CH_4 \rightarrow CH_3 + H$	CH_4	(1, 1)	2	1.50	1.09	10
	CH_3	(1, 0)	1			
	H	(1, 0)	1			
$NH_3 \rightarrow NH_2 + H$	NH_3	(1, 1)	2	1.50	1.01	8
	NH_2	(1, 0)	1			
	H	(1, 0)	1			
$CH_3F \rightarrow CH_3 + F$	CH_3F	(1, 1)	2	1.20	1.09	10
	CH_3	(1, 0)	1			
	F	(1, 0)	1			
$OH \rightarrow O + H$	OH	(3, 2)	4	1.50	0.98	8
	O	(3, 1)	3			
	H	(1, 0)	1			

Dissociation curve	Species	Number of electrons in active space (α, β)	Number of orbitals in active space	A	$D_{eq}(\text{\AA})$	n
$\text{CH}_3 \rightarrow \text{CH}_2 + \text{H}$	CH_3	(2, 1)	3	1.30	1.08	8
	CH_2	(2, 0)	2			
	H	(1, 0)	1			
$\text{NH}_2 \rightarrow \text{NH} + \text{H}$	NH_2	(2, 1)	3	1.30	1.03	8
	NH	(2, 0)	2			
	H	(1, 0)	1			
$\text{CH}_2 \rightarrow \text{CH} + \text{H}$	CH_2	(1, 1)	2	1.35	1.11	8
	CH	(1, 0)	1			
	H	(1, 0)	1			
$\text{NH} \rightarrow \text{N} + \text{H}$	NH	(3, 1)	4	1.20	1.04	8
	N	(3, 0)	3			
	H	(1, 0)	1			
$\text{CH}_3\text{Cl} \rightarrow \text{CH}_3 + \text{Cl}$	CH_3Cl	(1, 1)	2	1.35	1.79	8
	CH_3	(1, 0)	1			
	Cl	(1, 0)	1			
$\text{H}_2\text{S} \rightarrow \text{S} + 2\text{H}$	H_2S	(4, 4)	6	1.35	1.34	8
	S	(4, 2)	4			
	H	(1, 0)	1			
$\text{PH}_3 \rightarrow \text{P} + 3\text{H}$	PH_3	(3, 3)	6	1.35	1.42	12
	P	(3, 0)	3			
	H	(1, 0)	1			
$\text{HCN} \rightarrow \text{HC} + \text{N}$	HCN	(3, 3)	6	1.35	1.15	8
	HC	(3, 0)	3			
	N	(3, 0)	3			
$\text{NO} \rightarrow \text{N} + \text{O}$	NO	(5, 4)	7	1.20	1.14	8
	N	(3, 0)	3			
	O	(4, 2)	4			
$\text{CH}_3\text{OH} \rightarrow \text{CH}_3\text{O} + \text{H}$	CH_3OH	(1, 1)	2	1.50	0.96	8
	CH_3O	(1, 0)	1			
	H	(1, 0)	1			
$\text{CH}_3\text{OH} \rightarrow \text{CH}_2\text{OH} + \text{H}$	CH_3OH	(1, 1)	2	1.50	1.09	8
	CH_2OH	(1, 0)	1			
	H	(1, 0)	1			
$\text{CH}_3\text{OH} \rightarrow \text{CH}_3 + \text{OH}$	CH_3OH	(1, 1)	2	1.30	1.42	8
	CH_3	(1, 0)	1			
	OH	(1, 0)	1			

6. Supplementary References

- [1] Cleland, D.; Booth, G. H.; Overy, C.; Alavi, A., Taming the first-row diatomics: a full configuration interaction quantum monte carlo study. *J. Chem. Theory Comput.* **2012**, *8* (11), 4138-4152.
- [2] Peverati, R.; Truhlar, D. G., Quest for a universal density functional: the accuracy of density functionals across a broad spectrum of databases in chemistry and physics. *Philos. Trans. A Math. Phys. Eng. Sci.* **2014**, *372* (2011), 20120476.
- [3] Zhao, Y.; Tishchenko, O.; Gour, J. R.; Li, W.; Lutz, J. J.; Piecuch, P.; Truhlar, D. G., Thermochemical kinetics for multireference systems: addition reactions of ozone. *J. Phys. Chem. A* **2009**, *113* (19), 5786-5799.
- [4] Mardirossian, N.; Head-Gordon, M., Thirty years of density functional theory in computational chemistry: An overview and extensive assessment of 200 density functionals. *Mol. Phys.* **2017**, *115* (19), 2315-2372.
- [5] Goerigk, L.; Hansen, A.; Bauer, C.; Ehrlich, S.; Najibi, A.; Grimme, S., A look at the density functional theory zoo with the advanced GMTKN55 database for general main group thermochemistry, kinetics and noncovalent interactions. *Phys. Chem. Chem. Phys.* **2017**, *19* (48), 32184-32215.
- [6] Motta, M.; Ceperley, D.; Chan, G.; Gomez, J.; Gull, E.; Guo, S.; Jiménez-Hoyos, C.; Lan, T.; Li, J.; Ma, F.; Millis, A.; Prokofev, N.; Ray, U.; Scuseria, G.; Sorella, S.; Stoudenmire, E.; Sun, Q.; Tupitsyn, I.; White, S.; Zhang, S., Towards the Solution of the Many-Electron Problem in Real Materials: Equation of State of the Hydrogen Chain with State-of-the-Art Many-Body Methods. *Physical Review X* **2017**, *7*.
- [7] Zhang, I. Y.; Xu, X., Simultaneous Attenuation of Both Self-Interaction Error and Nondynamic Correlation Error in Density Functional Theory: A Spin-Pair Distinctive Adiabatic-Connection Approximation. *The Journal of Physical Chemistry Letters* **2019**, *10*, 2617-2623.
- [8] Weigend, F.; Furche, F.; Ahlrichs, R., Gaussian basis sets of quadruple zeta valence quality for atoms H-Kr. *J. Chem. Phys.* **2003**, *119*(1), 12753-12762.
- [9] Rappoport, D.; Furche, F., Property-optimized Gaussian basis sets for molecular response calculations. *J. Chem. Phys.* **2010**, *133*, 134105.
- [10] Frisch, M. J.; Trucks, G. W.; Schlegel, H. B.; Scuseria, G. E.; Robb, M. A.; Cheeseman, J. R.; Scalmani, G.; Barone, V.; Petersson, G. A.; Nakatsuji, H.; Li, X.; Caricato, M.; Marenich, A. V.; Bloino, J.; Janesko, B. G.; Gomperts, R.; Mennucci, B.; Hratchian, H. P.; Ortiz, J. V.; Izmaylov, A. F.; Sonnenberg, J. L.; Williams, J.; Ding, F.; Lipparini, F.; Egidi, F.; Goings, J.; Peng, B.; Petrone, A.; Henderson, T.; Ranasinghe, D.; Zakrzewski, V. G.; Gao, J.; Rega, N.; Zheng, G.; Liang, W.; Hada, M.; Ehara, M.; Toyota, K.; Fukuda, R.; Hasegawa, J.; Ishida, M.; Nakajima, T.; Honda, Y.; Kitao, O.; Nakai, H.; Vreven, T.; Throssell, K.; Montgomery Jr., J. A.; Peralta, J. E.; Ogliaro, F.; Bearpark, M. J.; Heyd, J. J.; Brothers, E. N.; Kudin, K. N.; Staroverov, V. N.; Keith, T. A.; Kobayashi, R.; Normand, J.; Raghavachari, K.; Rendell, A. P.; Burant, J. C.; Iyengar, S. S.; Tomasi, J.; Cossi, M.; Millam, J. M.; Klene, M.; Adamo, C.; Cammi, R.; Ochterski, J. W.; Martin, R. L.; Morokuma, K.; Farkas, O.; Foresman, J. B.; Fox, D. J. *Gaussian 16 Rev. C.01*, Wallingford, CT, 2016.
- [11] Sun, Q.; Zhang, X.; Banerjee, S.; Bao, P.; Barbry, M.; Blunt, N. S.; Bogdanov, N. A.;

- Booth, G. H.; Chen, J.; Cui, Z. H.; Eriksen, J. J.; Gao, Y.; Guo, S.; Hermann, J.; Hermes, M. R.; Koh, K.; Koval, P.; Lehtola, S.; Li, Z.; Liu, J.; Mardirossian, N.; McClain, J. D.; Motta, M.; Mussard, B.; Pham, H. Q.; Pulkin, A.; Purwanto, W.; Robinson, P. J.; Ronca, E.; Sayfutyarova, E. R.; Scheurer, M.; Schurkus, H. F.; Smith, J. E. T.; Sun, C.; Sun, S. N.; Upadhyay, S.; Wagner, L. K.; Wang, X.; White, A.; Whitfield, J. D.; Williamson, M. J.; Wouters, S.; Yang, J.; Yu, J. M.; Zhu, T.; Berkelbach, T. C.; Sharma, S.; Sokolov, A. Y.; Chan, G. K., Recent developments in the PySCF program package. *J. Chem. Phys.* **2020**, *153* (2), 024109.
- [12] Sun, Q.; Berkelbach, T. C.; Blunt, N. S.; Booth, G. H.; Guo, S.; Li, Z.; Liu, J.; McClain, J. D.; Sayfutyarova, E. R.; Sharma, S.; Wouters, S.; Chan, G. K.-L., PySCF: The Python-based simulations of chemistry framework. *WIREs Comput. Mol. Sci.* **2018**, *8* (1), e1340.
- [13] Sun, Q., Libcint: An efficient general integral library for Gaussian basis functions. *J. Comput. Chem.* **2015**, *36* (22), 1664-1671.
- [14] Liu, Y.; Zhang, C.; Liu, Z.; Truhlar, D. G.; Wang, Y.; He, X., Supervised learning of a chemistry functional with damped dispersion. *Nat. Comput. Sci.* **2023**, *3* (1), 48-58.
- [15] Kresse, G.; Hafner, J., Ab initio molecular dynamics for open-shell transition metals. *Phys. Rev. B* **1993**, *48* (17), 13115-13118.
- [16] Kresse, G.; Furthmüller, J., Efficiency of ab-initio total energy calculations for metals and semiconductors using a plane-wave basis set. *Comput. Mater. Sci.* **1996**, *6* (1), 15-50.
- [17] Kresse, G.; Furthmüller, J., Efficient iterative schemes for ab initio total-energy calculations using a plane-wave basis set. *Phys. Rev. B* **1996**, *54* (16), 11169-11186.
- [18] Blöchl, P. E., Projector augmented-wave method. *Phys. Rev. B* **1994**, *50* (24), 17953-17979.
- [19] Monkhorst, H. J.; Pack, J. D., Special points for Brillouin-zone integrations. *Phys. Rev. B* **1976**, *13* (12), 5188-5192.
- [20] Chen, B.; Xu, X., XO-PBC: An accurate and efficient method for molecular crystals. *J. Chem. Theory Comput.* **2020**, *16* (7), 4271-4285.
- [21] Guo, W.; Wu, A.; Zhang, I. Y.; Xu, X., XO: An extended ONIOM method for accurate and efficient modeling of large systems. *J. Comput. Chem.* **2012**, *33* (27), 2142-2160.
- [22] Chen, Z.; Liu, Z.; Xu, X., Accurate descriptions of molecule-surface interactions in electrocatalytic CO₂ reduction on the copper surfaces. *Nat. Commun.* **2023**, *14* (1), 936.
- [23] Weigend, F.; Ahlrichs, R., Balanced basis sets of split valence, triple zeta valence and quadruple zeta valence quality for H to Rn: Design and assessment of accuracy. *Phys. Chem. Chem. Phys.* **2005**, *7* (18), 3297-305.
- [24] Spencer, J. S.; Blunt, N. S.; Choi, S.; Etrych, J.; Filip, M.-A.; Foulkes, W. M. C.; Franklin, R. S. T.; Handley, W. J.; Malone, F. D.; Neufeld, V. A.; Di Remigio, R.; Rogers, T. W.; Scott, C. J. C.; Shepherd, J. J.; Vigor, W. A.; Weston, J.; Xu, R.; Thom, A. J. W., The HANDE-QMC project: Open-source stochastic quantum chemistry from the ground state up. *J. Chem. Theory Comput.* **2019**, *15* (3), 1728-1742.
- [25] Cleland, D.; Booth, G. H.; Alavi, A., Communications: Survival of the fittest: Accelerating convergence in full configuration-interaction quantum Monte Carlo. *J. Chem. Phys.* **2010**, *132* (4), 041103.
- [26] Neufeld, V. A.; Thom, A. J. W., Accelerating convergence in fock space quantum monte carlo methods. *J. Chem. Theory Comput.* **2019**, *16* (3), 1503-1510.
- [27] Yu, H.; Truhlar, D. G., What dominates the error in the CaO diatomic bond energy predicted by

various approximate exchange–correlation functionals? *J. Chem. Theory Comput.* **2014**, *10* (6), 2291-2305.

[28] Pedley, J. B.; Marshall, E. M., Thermochemical data for gaseous monoxides. *J. Phys. Chem. Ref. Data* **1983**, *12* (4), 967-1031.

[29] Yu, H. S.; Zhang, W.; Verma, P.; He, X.; Truhlar, D. G., Nonseparable exchange–correlation functional for molecules, including homogeneous catalysis involving transition metals. *Phys. Chem. Chem. Phys.* **2015**, *17* (18), 12146-12160.

[30] Curtiss, L. A.; Raghavachari, K.; Redfern, P. C.; Pople, J. A., Assessment of Gaussian-2 and density functional theories for the computation of enthalpies of formation. *J. Chem. Phys.* **1997**, *106* (3), 1063-1079.